



**The circular RNAs, *circPPP1R13B(2-4)* and  
*circNFASC(26,27)*, are upregulated in  
Glioblastoma and reduce cellular  
tumorigenicity**

**He Lin**

**Master of Biotechnology**

Thesis

Submitted to Flinders University for the degree of

**Master of Biotechnology**

Flinders Centre for Innovation in Cancer

College of Medicine and Public Health

May 2023

BMedSci

(Master)

College of Medicine & Public Health

FLINDERS UNIVERSITY

**Student Name**

He Lin

**Assignment**

Thesis

**Scientific Title**

The circular RNAs, *circPPP1R13B(2-4)* and *circNFASC(26,27)*, are upregulated in Glioblastoma and reduce cellular tumorigenicity

**Lay Title**

Effects of manipulating gene products in brain cancer cells

**Supervisor: Name and Department**

Prof Simon Conn

College of Medicine and Public Health; Flinders University

**Examiner 1: Name and Address**

Dr. Sunita Ramesh

College of Science and Engineering; Flinders University

**Examiner 2: Name and Address**

Dr. Amy Dwyer

Faculty of Health and Medical Sciences; University of Adelaide

**Due Date**

9<sup>th</sup> May 2023

## Table of Contents

<b>Abstract.....</b>	<b>7</b>
<b>Statement of Originality.....</b>	<b>8</b>
<b>Acknowledgement.....</b>	<b>8</b>
<b>Abbreviations .....</b>	<b>9</b>
<b>1. Introduction.....</b>	<b>10</b>
<b>1.1 Glioblastoma (GBM).....</b>	<b>10</b>
1.1.1 Prevalence.....	11
1.1.2 Current treatment and survival rate .....	11
1.1.3 New strategies for treatment.....	13
<b>1.2 Non-coding RNAs.....</b>	<b>13</b>
1.2.1 History of circRNAs .....	14
1.2.2 Location and stability of circRNAs .....	14
1.2.3 CircRNA biogenesis .....	15
1.2.4 Functions of circRNAs.....	17
<b>1.3 CircRNAs in the brain and central nervous system (CNS) .....</b>	<b>20</b>
1.3.1 circRNAs in GBM.....	21
<b>1.4 Application of circRNAs in GBM .....</b>	<b>22</b>
1.4.1 Biomarker.....	22
1.4.2 CircRNAs as therapeutic targets.....	24
<b>1.5 Strategies for overexpressing circRNAs.....</b>	<b>24</b>
1.5.1. Synthetic circRNAs .....	24
1.5.2. CircRNA overexpression vectors .....	25
<b>1.6 Project basis.....</b>	<b>26</b>

1.6.1 Project hypothesis.....	27
1.6.1 Project aims.....	27
<b>2. Materials and Methods .....</b>	<b>27</b>
<b>2.1 Analyses of RNA sequencing Data .....</b>	<b>28</b>
2.1.1. Estimation of differential expression.....	28
2.1.2 Primer design.....	28
<b>2.2 Cell culture.....</b>	<b>31</b>
2.1.1 Cell culture reagents.....	31
2.1.2 Cell Lines.....	32
2.2.1 Cell culture and passage.....	32
2.2.2 Freezing/ thawing cells.....	33
<b>2.3. RNA purification .....</b>	<b>33</b>
<b>2.4 Ribonuclease R (RNase R) treatment and purification.....</b>	<b>33</b>
<b>2.5 Complementary DNA (cDNA) synthesis.....</b>	<b>34</b>
<b>2.6 Polymerase chain reaction (PCR).....</b>	<b>34</b>
<b>2.7 Agarose Gel Electrophoresis and Gel extraction .....</b>	<b>34</b>
<b>2.8 Sanger sequencing .....</b>	<b>35</b>
<b>2.9 Quantitative real-time RT-PCR.....</b>	<b>35</b>
<b>2.10 Transfection of cell lines .....</b>	<b>35</b>
2.10.1 Plasmid extraction and digestion.....	35
2.10.2 Cloning and bacterial transformation.....	36
2.10.4 Screening bacterial colonies.....	37
2.10.5 Transient transfection.....	37
2.10.6 Gradient PCR.....	37
2.10.7 Nuclear:cytoplasmic fractionation.....	38

2.10.8 Transfection U251 and U87 cell lines .....	38
<b>2.11 Cell assays .....</b>	<b>39</b>
2.11.1 Cell growth rate analysis .....	39
2.11.2 Cell size and shape analysis.....	39
2.11.3 Colony Formation Assay .....	40
<b>2.12 Protein analysis .....</b>	<b>41</b>
2.12.1 Protein extraction .....	41
2.12.2 Bradford protein quantification assay .....	42
2.12.3 Western blotting .....	42
<b>3. Results .....</b>	<b>43</b>
<b>3.1 Analysis of RNAseq Data for candidate selection .....</b>	<b>43</b>
3.1.1. Estimated differential expression between GBM and non-tumour tissue .....	43
3.1.2. Selection of circRNA candidates .....	43
<b>3.2. Validation of primers for circRNA candidates.....</b>	<b>45</b>
3.2.1. PCR validation of circRNA Primers .....	45
3.2.2. Sequencing of PCR products.....	47
<b>3.3 Selection of circRNA candidates .....</b>	<b>48</b>
<b>3.4 Overexpressing circRNA candidates .....</b>	<b>48</b>
3.4.1. Plasmid digestion.....	48
3.4.2. Gibson assembly and colony PCR.....	49
3.4.4. Transient transfection.....	50
3.4.5 RNase R resistance of circRNA.....	52
3.4.6 Stable CircRNA overexpression.....	53
3.4.7 Western blot to detect KCNN2 protein .....	56
3.4.8 qRT-PCR validation of nuclear/cytosolic fractionation.....	58

<b>3.5 Cell assays .....</b>	<b>59</b>
3.5.1 Cell proliferation .....	59
3.5.3 Cell morphology .....	62
3.5.4 miRNA prediction .....	64
3.5.5 CircRNA database analysis .....	66
<b>4. Discussion .....</b>	<b>67</b>
<b>5. Limitations of this study.....</b>	<b>70</b>
<b>6. Future directions.....</b>	<b>71</b>
<b>Appendix O.....</b>	<b>73</b>
<b>Appendix I.....</b>	<b>74</b>
<b>Appendix II.....</b>	<b>75</b>
<b>Appendix III.....</b>	<b>77</b>
<b>Appendix IV.....</b>	<b>78</b>
<b>Appendix V.....</b>	<b>79</b>
<b>Appendix VI.....</b>	<b>79</b>
<b>Appendix VII.....</b>	<b>80</b>
<b>Appendix VIII.....</b>	<b>80</b>
<b>7. References.....</b>	<b>81</b>

## Abstract

Patients with glioblastoma (GBM), the most common malignant brain tumour, have a median survival of 12-15 months after diagnosis, with less than 5% of patients surviving 5 years. While the average survival rate of most cancers has improved by ~20% in the past 30 years, survival from GBM has not improved. Therefore, a deeper fundamental understanding of GBM is required for identifying the disease at an earlier stage and for identifying targets for more effective therapies. Circular RNAs (circRNAs) are the most contemporary family of largely non-coding RNA molecules which are particularly abundant in brain tissue. CircRNAs arise from alternative splicing of pre-mRNA transcripts and have been shown to be functional molecules offering potential as both cancer biomarkers and therapeutic targets.

Our laboratory has previously profiled circRNAs by high-throughput RNA-seq on five healthy brain tissue samples and five GBM tumours. From over 72,000 high confidence circRNAs in this dataset, 5,366 circRNAs showed > 2-fold differential expressions between the tissue with 3,647 circular RNAs downregulated in GBM. The hypothesis of this project is that overexpression of circRNAs downregulated in GBM can affect the oncogenic characteristics of GBM cell lines. The aims of the project were to (1) Identify candidate circRNAs which are downregulated in GBM tumours compared with control healthy brain tissue, (2) Generate GBM cell lines stably overexpressing candidate circRNAs and (3) Assess phenotypes in circRNA overexpressing GBM cell lines

By transgenically overexpressing three downregulated circRNAs, *circPPP1R13B(2-4)*, *circKCNN2(8)* and *circNFASC(26,27)* in the two most widely used GBM cell lines (U87 and U251) their effects on molecular and cellular biology was investigated. Despite showing no effect on cell proliferation, overexpressing *circPPP1R13B(2-4)* in U251 cells and overexpressing *circNFASC(26,27)* in U87 cells was shown to reduce the tumorigenicity *in vitro* using a colony formation assay by 36% and 29%, respectively. High-content fluorescence microscopy was performed to study cellular and nuclear morphology which are known to be distorted in a number of cancers. Cell morphology assay shows *circKCNN2(8)*

increased cell size by 37% in U87 cells, and overexpressing *circNFASC(26,27)* in U87 cells increased both nucleus and cell areas by 27% and 64%, respectively.

The results of this project indicate that circRNAs can change the phenotypes of GBM cells. Exploring more circRNAs is worthwhile because they have the potential to reduce the tumorigenicity of GBM cells, thus leading us into a new era in the treatment of GBM.

## **Statement of Originality**

I certify that this thesis does not incorporate without acknowledgment any material previously submitted for a degree or diploma in any university; and that to the best of my knowledge and belief it does not contain any material previously published or written by another person except where due reference is made in the text.

He Lin

9th May 2023

## **Acknowledgement**

Firstly, I would like to thank my supervisor, Prof Simon Conn, for taking me on as his master's student this year and being a wonderful mentor. I am really grateful for all the help you have given me this year, especially for encouraging me when I lose some motivation and guiding me through the entire project.

Secondly, I would like to thank my examiners, Dr. Sunita Ramesh and Dr. Amy Dwyer, for volunteering their time to evaluate my work and provide insightful and valuable feedback. I am extremely grateful for your efforts.

I would also like to thank members of my laboratory, Dr. Vanessa Conn, Dr. Brett Stringer, Dr. Stuart Webb, Kirsty Kirk, Laura Gantley, and Ryan Liu for giving constant support and answering my questions throughout my research.

Finally, I would like to thank my family and my husband, Jingyun Guo, for being such a powerful network outside the lab. Without you, I would not have made it through this year.

## **Abbreviations**

ADAR1: RNA-specific adenosine deaminase 1

BHB: bulge-helix-bulge

CDK2: cyclin-dependent kinase 2

circRNA: circular RNA

CNS: central nervous system

CSF: cerebrospinal fluid

CT: computed tomography

dsRNA: double-stranded RNA

EcRNA: extra coding RNA

EV: empty vector

GBM: Glioblastoma

ICIs: immune checkpoint inhibitors

IRES: internal ribosome entry site

M6A: N<sup>6</sup>-Methyladenosine

MBL: Muscleblind

MGMT: Methylguanine methyltransferase

miRNA: micro-RNA

MRI: magnetic resonance imaging

ncRNA: non-coding RNA

NTC: none template control

OEX: overexpression

pol II: RNA polymerase II

QKI: Quaking

RBPs: RNA-binding proteins

RNAi: RNA interference

shRNA: short hairpin RNA

siRNA: short interfering RNA

TMZ: temozolomide

## **1. Introduction**

### **1.1 Glioblastoma (GBM)**

A brain tumour is an abnormal growth of brain tissues. There are two main types of brain tumours, which are termed primary and secondary (also known as metastatic) (Gabriela Pichardo, 2020). Primary brain tumours, which start in the brain and rarely spread to other parts of the body, can be categorised as benign and malignant (Gabriela Pichardo, 2020). Secondary brain tumours are caused by cancers that arise in other parts of the body (such as the breast and lungs) and migrate to the brain. Gliomas account for 75% of malignant primary brain tumours (Lv et al., 2022). They originate from the brain-supporting cells, called glial cells (Gabriela Pichardo, 2020), with astrocytes, ependymal cells, and oligodendroglial cells being the three different types of glial cells (Gabriela Pichardo, 2020). Gliomas are classified into four grades (I, II, III, and IV), with grade I being the least aggressive and grade IV being

the most aggressive (Marquet et al., 2007). Grade IV glioma, also called glioblastoma (GBM), is the most common and aggressive malignant primary brain tumour of the central nervous system (CNS) (Tan et al., 2020). GBM is highly heterogeneous and comprises different cell types, such as astrocytes and oligodendrocytes. GBM accounts for around 57% of all gliomas and 48% of CNS cancers (Ostrom et al., 2018). While considered a rare cancer, it kills the greatest number of people under the age of 40 of any disease and it is currently incurable.

### 1.1.1 Prevalence

The incidence of GBM ranges from 0.59 to 5 per 100,000 population, and it is increasing in many countries (Grech et al., 2020). In Australia, the age-adjusted incidence rate of GBM is 3.4 per 100,000 population in 2014, while in 2022, it increased by over 40% to 4.8 per 100,000 population (Ostrom et al., 2014, Alpen et al., 2022). The reasons for the increasing incidence are unknown, the contributing factors are the increase in diagnosis technologies, air pollution, and an aging population, among others (Grech et al., 2020). The global different incidence of GBM is caused by many reasons, and one of the most significant factors is the variation in health infrastructure and cancer registration systems (Leece et al., 2017). Middle- or low- countries have less access to imaging technologies such as CT, MRI and X-ray, leading to underdiagnosis rather than truly lower incidence. Variation in health systems affects whether the diagnosis of brain tumours is reported to cancer registry systems. There is also a gender bias, with increased incidence in males than in females. In Australia, the annual age-adjusted incidence in males is 1.4 times that in females (Alpen et al., 2022).

### 1.1.2 Current treatment and survival rate

The current standard-of-care treatment for GBM includes surgery, radiotherapy, chemotherapy, and supportive care. If feasible, maximal safe surgical resection is the guiding principle for GBM, followed by radiotherapy and temozolomide (TMZ) (Tan et al., 2020). TMZ is an oral alkylating agent used to treat GBM, but it is not as effective in people with O<sup>6</sup>-methylguanine methyltransferase (MGMT) promoter (Lee, 2016). In 2005, the Stupp protocol became the standard care for treating GBM, which consists of radiotherapy and

chemotherapy with TMZ (Stupp et al., 2005). Standard radiotherapy delivers a total of 60 Gray over 6 weeks in 30 fractions, in combination with TMZ (Stupp et al., 2005). During radiotherapy, the dose of TMZ is 75 mg/m<sup>2</sup> (Stupp et al., 2005). In the adjuvant therapy period, temozolomide is increased to 150-200 mg/m<sup>2</sup> for 6 cycles, 28 days/cycle (Stupp et al., 2005). The use of TMZ can have some toxic effects, such as thrombocytopenia and neutropenia, and they are common side effects during TMZ chemotherapy period. In Australia, in addition to traditional TMZ, lomustine, bevacizumab, procarbazine, carboplatin and etoposide are other salvage options (Sim et al., 2020). Patients with GBM commonly have severe and progressing neurologic symptoms that can interfere with their functioning and regular life activities (McKinnon et al., 2021). Therefore, higher levels of nursing and supportive care are necessary.

Although extensive therapies are available, the median survival is 12-15 months after diagnosis, with less than 5% of patients surviving 5 years (Delgado-López and Corrales-García, 2016). While there has been an increase in survival from most cancers in the past 30 years, including prostate and breast cancer, survival from GBM has not improved significantly over the past 3 decades (**Fig.1**) (Health and Welfare, 2022). Therefore, it is urgent to find new strategies for both therapy and prognosis to increase the survival rate and quality of life.

Figure removed due to copyright restriction

**Figure 1: Comparison of survival rates of prostate and brain cancers from 1989-2018**  
(Health and Welfare, 2022)

### 1.1.3 New strategies for treatment

Immunotherapy is a revolution in cancer treatment, in which the use of immune checkpoint inhibitors (ICIs) has been clinically effective, for example in improving the outcome of non-small-cell lung cancer (Luke et al., 2017). This therapy primarily relies on the capability of T-cell infiltration to recognise and kill tumour cells, however, GBM is characterised by a lack of T-cell infiltration, so ICIs are not effective in the treatment of the GBM (Liu and Sun, 2021). Tumours can be classified as ‘hot’ or ‘cold’ tumours according to their responses to immunotherapy. With the deeper study of GBM, many results suggest that it is a cold tumour (Lim et al., 2018). Although the results of current immunotherapy trials have been disappointing, the conversion of GBM from cold to hot tumours followed by immunotherapy combined with current treatment protocols may provide hope for a new therapy.

The lack of biomarkers is another big challenge in immunotherapy for GBM. The gold standard for assessing disease status is Magnetic Resonance Imaging (MRI), but the challenge with this method is discriminating pseudo-progression and pseudo-response (Da Cruz et al., 2011, Ryken et al., 2014). Furthermore, repeat sampling by biopsy or surgical excision carries as much risk as surgery. Therefore, finding validated biomarkers in the circulation not only helps in the early diagnosis of the disease but also its treatment, resulting in improvements in outcomes of GBM.

## 1.2 Non-coding RNAs

Only ~2% of the human genome comprises protein-coding genes, with the remainder inaptly referred to as “junk” DNA. Unsurprisingly, this remaining vast landscape has been shown to play critical functions in cells and encode for non-translated RNAs, called non-coding RNAs. The most recently discovered family of largely non-coding RNAs are circular RNAs (circRNAs). CircRNAs not only play an important role in normal cell functions but also in cancer growth and development because they can regulate transcription, splicing and translation (Djebali et al., 2012, Goodall and Wickramasinghe, 2021). Some ncRNAs can be used as targets for drugs to treat diseases. For example, strategies to increase or decrease microRNA expression levels to treat cancer are already in clinical trials (Seto et al., 2018).

CircRNAs are found across all kingdoms of life, with each eukaryotic cell able to express a unique repertoire of thousands of circRNAs at varying levels of expression (Salzman et al., 2012). More than 1,000,000 different circRNAs have been identified through RNA sequencing, which can be found across a number of circRNA online databases (Vo et al., 2019). Some circRNAs have been found to be cell-type specific and also disease-specific, while others show different expression levels in cancers compared with the respective normal tissues. As circRNAs are very stable, they are considered ideal biomarkers for the diagnosis of cancers. CircRNAs have been detected in the majority of body fluids, including circRNAs in the urine of prostate cancer patients (Vo et al., 2019). CircRNAs also play a crucial role in GBM, not only as potential biomarkers but their expression has also been linked to the course and recurrence of the disease (Salami et al., 2022).

### 1.2.1 History of circRNAs

CircRNAs were first discovered in pathogens in 1972, being found in human cells seven years later (Hsu and Coca-Prados, 1979). Since then, circRNAs have been found in a variety of species, including viruses, prokaryotes, unicellular eukaryotes, and mammals (Zhou et al., 2020). By the early 2010s, research on circRNAs had expanded with the development of bespoke bioinformatics pipelines matched with RNA sequencing technologies. Scientists have identified over 1 million circRNAs, and studies have shown links between circRNAs and cancers (Kristensen et al., 2018).

### 1.2.2 Location and stability of circRNAs

Most circRNAs are enriched in the cytoplasm, with intron-containing circRNAs found to be more abundant within the nucleus (Li et al., 2015). UAP56/URH49 are important circRNA localisation modulators that regulate nuclear export effectiveness in a circRNA size-dependent manner (Huang et al., 2018). CircRNAs have an average half-life of 19 to 24 hours, greatly exceeding the half-life of cognate mRNA molecules of a few minutes up to 9 hours (Holdt et al., 2018). Exonucleases, including ribonuclease R (RNase R), which digest from the termini of linear RNA, are unable to degrade circRNAs, contributing to their

increased half-lives (Zhang et al., 2020). For this reason, some circRNAs can be detected at levels above their parent mRNA, though the vast majority are comparatively lowly expressed (Zhang et al., 2020).

### 1.2.3 CircRNA biogenesis

CircRNAs are formed by non-canonical splicing events, known as backsplicing (**Fig. 2**). Unlike pre-mRNAs which are canonically spliced in the 5' to 3' direction of the RNA molecule, backsplicing occurs from the 3'-end of a downstream exon (splice donor site) to the 5'-end of an upstream exon (splice acceptor site) (Conn et al., 2020). The uniqueness of this novel junction site, called a backsplice junction, allows it to be identified from high throughput RNA sequencing, amplified across with divergent oligonucleotide primers, or targeted by RNA interference strategies independent of the linear RNA (Kristensen et al., 2019). This process is guided by the spliceosome, as well as cis-acting elements and trans-acting factors (Li et al., 2020). Most circRNAs contain single or multiple exons, some of them contain both exons and introns, and some only contain introns (Kristensen et al., 2019).

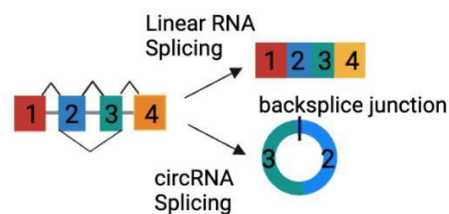


**Figure 2: Linear and circular RNA splicing.** Linear RNA is formed from pre-mRNAs by intron removal and exon splicing from 5' to 3' direction, while circRNA splicing involves the splicing of a downstream splice site to an upstream splice site producing a backsplice junction (shown between exons 2 and 3). Squares with numbers are exons, and the image was created by BioRender.com.

The complementary sequences in introns flanking the exons are the crucial *cis*-acting elements for the formation of circRNAs because this complementary pairing will form a hairpin structure and bring the 5' splice-donor sites and 3' splice-acceptor sites into close proximity to encourage backsplicing (**Fig. 3A**). *Alu* repeats (short repetitive elements) are commonly involved within these complementary sequences, but these sequences can also be

nonrepetitive elements and short, as little as 10-25 nucleotides in length (Zhang et al., 2014). Circularization that is driven by *Alu* repeats is more complex because *Alu* repeats can be in different introns of one gene, leading to the formation of a variety of circRNAs from one gene. But not all introns containing *Alu* repeats will support the formation of circRNAs, and some short regions (<100 nucleotides) within *Alu* repeats can even suppress the circulation (Liang and Wilusz, 2014).

CircRNA biogenesis can also be regulated by specific RNA-binding proteins (RBPs), and these RBPs are identified as *trans*-acting elements (Li et al., 2020). For instance, Quaking (QKI), a nuclear protein, can recognise specific sequences in introns and then dimerise to make a bridge, thereby co-localising splice sites (**Fig. 3A, right**) (Conn et al., 2015), which promotes circRNA production. Other RBPs that can promote circRNA biogenesis are muscleblind (MBL), FUS and SRRM4 (Conn et al., 2020). However, some RBPs can suppress the formation of circRNAs by disrupting the base pairs in intron regions. For example, RNA-specific adenosine deaminase 1 (ADAR1) can prevent introns from complementary base pairing and reduce circRNA biogenesis (Wang et al., 2020).

Lariat-driven circularization is another model for circRNA biogenesis. It is also known as the exon-skipping or intron removal mechanism. In exon-skipping events, the skipped exons and introns will form a lariat loop (**Fig. 3B, left**). In intron removal events, circRNAs only containing introns are formed (**Fig. 3B, right**). This process relies on 7-nt GU rich sequences near the 5' splice site and 11-nt rich sequences near the branch point. The branch point is another sequence located anywhere from 18 to 40 nucleotides upstream from the 3' end of an intron (Clancy, 2008).

All exon-derived and exon-intron-derived circRNAs are from pre-mRNAs, but not all intronic-derived circRNAs come from pre-mRNAs. A small fraction of intronic-derived circRNAs is generated from pre-tRNAs. With the maturation of tRNAs, the canonical bulge-helix-bulge (BHB) will be cut, resulting in the formation of circRNAs, called tricRNAs (**Fig. 3C**)(Lu et al., 2015).

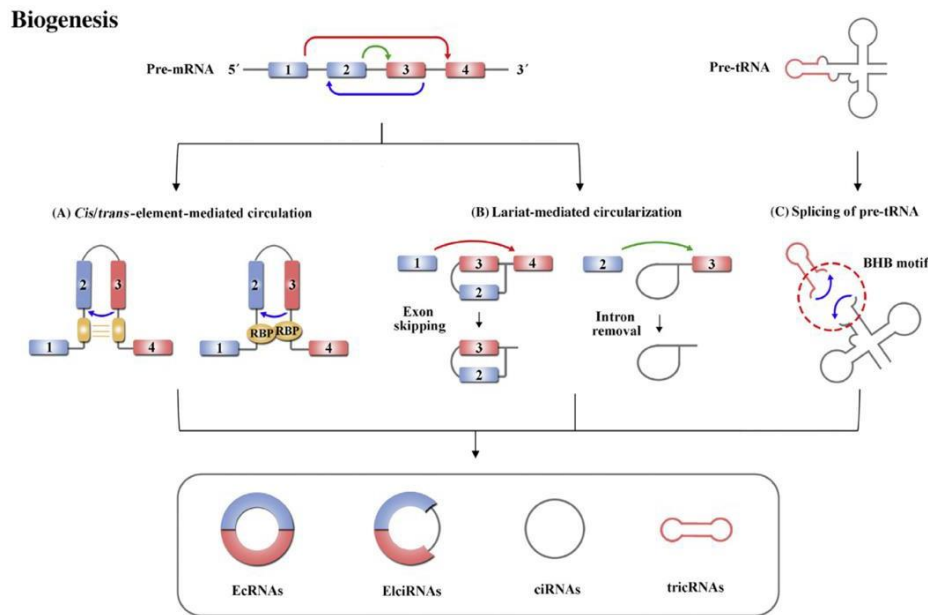


**Figure 3: Mechanisms of circRNA biogenesis** (Li et al., 2020). **A)** *Cis/trans* -elements, the complementary sequences in introns flanking the exons or RBPs, mediated the circularisation of circRNAs. **B)** Skipped exons and introns or introns form a lariat loop. **C)** CircRNAs are formed by BHB cut with the maturation of tRNAs. (RBPs: RNA-binding proteins; BHB: bulge-helix-bulge). Reprinted with permission from Trends in Cancers.

#### 1.2.4 Functions of circRNAs

In addition to back-splicing itself which will compete with canonical splicing, circRNAs have been reported to have other functions. They can not only regulate gene translation and transcription but also as micro-RNA (miRNA) sponges, and some of the circRNAs can interact with proteins (**Fig. 4**) (Zhou et al., 2020).

Figure removed due to copyright restriction

**Figure 4: Functions of circRNAs.** **a)** circRNAs can bind to their host gene, and form an R-loop structure, resulting in exon-skipped or truncated transcripts. **b)** circRNAs can enhance their parental gene expression by binding U1 snRNP, and then interacting with Pol II. **c)** circRNAs can act as miRNA sponges and upregulate miRNA target mRNA. **d)** CircRNAs can interact with proteins. **e)** circRNAs containing IRES can directly recruit ribosomes and initiate transcription. **f)** circRNAs containing m6A can be recognised by YTHDF3, which interacts with eIF4G2, thus starting translation. This process can be enhanced by Mett13/14 and suppressed by FTO. Figure reproduced from (Zhou et al., 2020)

#### 1.2.4.1 Regulating transcription

CircRNAs can alter gene expression by pausing or promoting gene transcription. In *Arabidopsis thaliana*, exon 6 of *SEPALLATA3* can be transcribed to an EcRNA, called *circSEP3*, which can bind with its cognate DNA (Conn et al., 2017). This binding will create an RNA-DNA hybrid, or R-loop, which impacts transcription (**Fig. 4a**), resulting in an alternatively spliced *SEP3* mRNA and the driving of a mutant flower phenotype in these plants (Conn et al., 2017). *CircSMARCA5* is another example which can form an R-loop at exon15 of *SMARCA5*, resulting in truncated transcription (Conn et al., in press). Introns in EiCiRNAs can bind with U1-specific ribonucleoprotein particles in small nuclear RNA (snRNA) by RNA-RNA interaction and then interact with RNA polymerase II (pol II) at the promoter region of parental genes, enhancing gene transcription (**Fig. 4b**) (Li et al., 2015). Likewise, intron-only circRNAs (ciRNAs) can also directly bind and activate Pol II to promote broader gene transcription (Zhang et al., 2013).

#### 1.2.4.2 MicroRNA sponge

MicroRNAs (miRNAs) are small, non-coding RNAs, which are important regulators of post-transcriptional gene expression. CircRNAs can act as miRNA sponges by binding them through complementary base-pairing which then affects the ability of the miRNAs to impact their network of target transcripts (**Fig. 4c**) (Zhang et al., 2013). *CDRIas* (also known as ciRS-7) is a notable example as it contains more than 70 conserved miR-7 binding sites, which results in increased expression of the miR-7 target mRNA network (Hansen et al., 2013, Memczak et al., 2013). However, *CDRIas* can also suppress the expression of genes that respond to different types of early stimuli by stabilising the miR-7 (Piwecka et al., 2017). By sequestering the miR-7 orthologue, *CDRIas* expressed in zebrafish was shown to regulate midbrain development (Memczak et al., 2013). Apart from *CDRIas*, *circHIPK2* is another example, which can act as a sponge for miR124-2HG and activate astrocytes, which then regulate cell proliferation (Ren et al., 2022).

#### 1.2.4.3 Interaction with proteins

Many studies have reported circRNAs can interact with proteins and function as protein scaffolds (**Fig. 4d**) (Huang et al., 2020). In different circumstances, one circRNA may bind one protein or multiple proteins, resulting in changing protein-protein interaction. There are two modes to explain circRNA-protein interactions: (1) both proteins bind to one circRNA, or (2) when a single protein binds to a circRNA, the interaction with protein B (not binding the circRNA) will be strengthened or inhibited (Zhou et al., 2020). An example of mode (1) involves *circFoxo3* and cell cycle proteins cyclin-dependent kinase 2 (CDK2) and cyclin-dependent kinase inhibitor 1 (P21) (Du et al., 2016). This binding forms the *circFoxo3*-p21-CDK2 ternary complex which inhibits the function of CDK2, which is normally responsible for cell cycle expression (Du et al., 2016). A highly cited example of the second mode involves *circCcnb1* (Fang et al., 2018). In p53 wild-type cells, *circCcnb1* can bind wild-type p53 via H2A.X histone variant facilitating p53 wild-type cell proliferation. In p53 mutant cells, *circCcnb1* can form a complex with H2A.X and Bclaf1, which can cause p53 mutant cell death, however, *CircCcnb1* must bind with p53 or Bclaf1 by H2AX, and cannot directly induce death of p53 mutant cells.

#### 1.2.4.4 Translation into protein

Ribosomes are necessary for mRNA translation because they can scan the mRNA from the 5'-cap to the 3'-end to find the start codon. There is no 5'-cap or 3'-polyA-tail in circRNAs, but certain circRNAs contain an internal ribosome entry site (IRES) that can directly recruit ribosomes (**Fig. 4e**). The resultant protein synthesis can proceed across the circRNA backsplice junction yielding novel protein sequence. Therefore, each circRNA molecule has higher productivity than their linear mRNA form. However, the majority of peptides encoded by circRNAs are truncated, and most of them have similar functions to their full-length protein counterparts. However, some proteins deriving from circRNAs have different functions compared to their host gene products. *CircFNDC3B* was reported to encode a novel protein (CircFNDC3B-218aa), which could be a suppressive factor in colon cancer (Pan et al., 2020).

The translation can be modified by N<sup>6</sup>-Methyladenosine (m6A), an RNA modification (**Fig. 4f**). According to one study, the translation of m6A-containing circRNAs can be driven by the interaction between YTHDF3 and eIF4G2, and this process can be enhanced by Mettl13/14 and suppressed by obesity-associated protein (FTO) (Yang et al., 2017).

### 1.3 CircRNAs in the brain and central nervous system (CNS)

Alternative splicing is a frequent occurrence in brain tissues and plays a role in all stages of nervous system development, including cell-fate decisions, neuronal migration, synaptogenesis and axon guidance (Su et al., 2018). CircRNAs are formed by alternative splicing, accordingly, circRNAs are more abundant in the brain than in other organs (You et al., 2015). Several studies have shown that circRNAs are important to CNS development, and many brain-enriched circRNAs are related to the neural plasticity (You et al., 2015). Neural plasticity is the ability of the nervous system to modify itself functionally and structurally in response to injury, environmental change and aging and this ability is at its peak in adults (Bernhardi et al., 2017). This change in brain plasticity is correlated with the abundance of circRNAs in the brain because, in human embryonic development, there were around 6,000

circRNAs detected in the brain, however, around 65,000 circRNAs were found in the adult brain (Chen et al., 2019). Some circRNAs have been reported to regulate brain plasticity, for example, *circHomer1* can modulate synaptic structural change during neuronal plasticity and development (You et al., 2015).

CircRNAs are not expressed at the same level in different regions of the brain, and region-specific circRNAs exist in the prefrontal cortex, olfactory bulb, cerebellum and hippocampus in the mouse brain (Salami et al., 2022). This neurospecificity of circRNAs may be due to their host genes being expressed differently in brain tissues, such as *HOMER1*, *RTN4* and *NTRK2* (Maass et al., 2017), and/or by protein biogenesis factors having cell type specific expression patterns.

### 1.3.1 circRNAs in GBM

The unusual expression of circRNAs in brain tissues is associated with the pathogenesis of neurological diseases, such as Alzheimer's disease (AD), Parkinson's disease (PD) and GBM (Floris et al., 2017). In Prof. Conn's lab, over 82,050 circRNAs have been identified by analysing five patients with grade II, III or IV glioma and matched healthy brain tissue. Comparing healthy tissue with GBM patients, 5,366 circRNAs have been found with different expressions in healthy brain tissues and GBM tumours: 3,647 circular RNAs are downregulated in GBM, and 1,719 circular RNAs are upregulated in GBM. With this dataset, a unique characteristic of circRNAs, the inclusion of very short exons (3-30 nucleotides (nt) in length) called microexons (ME-circRNAs), was identified (Conn et al., 2020). The expression of ME-circRNAs is regulated by serine/arginine repetitive matrix 4 (*SRRM4*), a splicing-associated factor, and is related to poor prognosis in gliomas (Conn et al., 2020).

CircRNAs can regulate GBM cell proliferation, differentiation and migration, through a variety of signalling pathways, including PI3K/Akt/mTOR, Wnt/ $\beta$ -catenin, MAPK and metastatic pathway (**Fig.5**) (Salami et al., 2022). For example, it has been demonstrated that hsa-circ-0067934, produced from the chromosomal region 3q26, is overexpressed in GBM

tissues and contributes to the course of the disease by promoting both proliferative and metastatic processes through the activation of PI3K/Akt signaling (Xin et al., 2019). It has been proposed that hsa-circ 0067934 could be used as a potential prognostic biomarker to identify GBM patients with higher specificity using a liquid biopsy. Furthermore, *circNT5E* has been shown to induce GBM cell proliferation, migration, invasion and subsequent inhibition of apoptotic flux by regulating the PI3K/Akt/mTOR signalling (Xin et al., 2019).

Figure removed due to copyright restriction

**Figure 5: The importance of CircRNAs and their impact on the progression of glioblastoma.** CircRNAs in the orange background can down-regulated GBM progression, and others can up-regulated GBM progression (Salami et al., 2022).

## 1.4 Application of circRNAs in GBM

### 1.4.1 Biomarker

The ability to cure cancer is greatly increased if the malignancy is discovered at an earlier stage (Shafabakhsh and Asemi, 2019). The current cancer diagnosis techniques including computed tomography (CT) scan, magnetic resonance imaging (MRI), and histology, are

invasive, expensive and open to interpretation (Salami et al., 2022). Due to the heterogeneity of the cells and numerous genetic mutations, the molecular aetiology of GBM is extremely complex. Therefore, it can be beneficial to search for diagnostic and prognostic biomarkers in bodily fluids and malignant tissue. Numerous biological specimens, such as blood samples, cerebrospinal fluid (CSF), urine, saliva, breast milk, different tissues, and exosomes, have been found to contain circRNAs (Zhang et al., 2020). In addition to the prevalence of cell-type-specific and disease-specific circRNAs, their covalently-closed structure affords them greater stability and longer half-lives than linear RNA. Therefore, circRNAs offer great potential as liquid biomarkers for diagnostic purposes in GBM patients.

It has been demonstrated that in GBM cell lines and tissues, hsa-circ-0043278, circ-PITX1, and circ-0074027 are considerably up-regulated, making them potential biomarkers for both the diagnosis and prognosis of GBM (Salami et al., 2022). Furthermore, the expression of circ-0001649 was strongly negatively correlated with tumour size and WHO grade, with overexpression of circ-0001649 encouraging apoptosis. This raises the possibility that circRNAs could act as independent and functional prognostic markers after commencing treatment (Wang et al., 2018).

Peptides and proteins that are encoded by circRNAs have recently been recognised as potential biomarkers for the diagnosis of GBM. The expression level of SHPRH-146aa, which is encoded by circ-SHPRH, is significantly higher in healthy human brain tissue than in GBM (Wu et al., 2021). By preventing the full-length SHPRH from DTL-induced ubiquitination, this new protein increases the half-life of the protein and activates its tumour-suppressive properties (Begum et al., 2018). Another protein in this classification is SMO-193aa, encoded by circ-SMO. It is necessary for the activation of hedgehog signalling and encourages cell proliferation, tumorigenicity, and self-renewal activities (Salami et al., 2022). Patients' short lifetimes are adversely correlated with SHPRH-146aa overexpression and SMO-193aa silencing, demonstrating the clinical use of these circRNA protein products.

### 1.4.2 CircRNAs as therapeutic targets

It has been demonstrated that some circRNAs can change important biological functions of GBM, including cell division, cell death, migration, invasion, and metastasis (Xiao et al., 2021). Therapeutic approaches that target circRNAs, therefore, constitute a novel approach to treating GBM. Circ-0001946 has a low expression level in GBM cells, and its overexpression reduced cell proliferation, migration, and invasion and increase apoptosis in GBM cells by circ-000194/miR-671-5p/*CDR1* pathway (Li and Diao, 2019), so circ-0001946 becomes an interesting target for treating GBM because of its anti-cancer properties. Therefore, increasing the expression of Circ-0001946 is one possible approach to slow GBM progression.

In GBM, a few circRNAs are upregulated and increase oncogenicity. For instance, the highly expressed *circFOXO3* can promote GBM cell proliferation and invasion (Zhang et al., 2019). Circular E-cadherin (circ-E-Cad), which encodes the oncogenic form of E-cadherin, is considerably overexpressed in GBM, promoting GBM tumorigenicity (Gao et al., 2021). It might be able to exploit oncogenic circRNAs as therapeutic targets if their expression is suppressed.

TMZ is the frontline chemotherapy for GBM patients after surgery to reduce the recurrence of GBM and prolong the patient's life. However, some tumours are resistant to TMZ, which reduces the effectiveness of treatment. *CircMTO1* was reported to be overexpressed in TMZ-resistant GBM cells and tissues (Zhu and Liu, 2019). Additional research showed that miR-630 was a target of *circMTO1* in GBM cells, and its knockdown decreased the resistance to TMZ. Therefore, by controlling miR-630, *circMTO1* can sensitise GBM cells to TMZ, offering a new and viable target for treating GBM.

## 1.5 Strategies for overexpressing circRNAs

### 1.5.1. Synthetic circRNAs

In addition to employing plasmids to increase circRNA expression, circRNAs can be overexpressed through direct synthesis and purification. Circularization of RNA can be

achieved via a variety of techniques (Müller and Appel, 2017), for example, splint ligation is the method that can be used to cyclize single-stranded, linear RNA from *in vitro* transcribed RNA. CircRNA molecules made using this method are extremely pure, and then can be delivered to target cells (Chen et al., 2019). However, the challenge of this approach is that cannot establish cell lines stably expressing the circRNA, which is diluted by cell proliferation and circRNA degradation.

### 1.5.2. CircRNA overexpression vectors

For achieving circulation, inserting *cis/trans*-acting factors and RNA-binding proteins for Quaking into constructed plasmids is a classic method for overexpressing circRNAs (Conn et al., 2015). In addition, a tRNA-based splicing mechanism is also used to overexpress circRNAs (Schmidt et al., 2016). Most commonly, overexpression of circular RNAs is achieved by cloning the circRNA sequence into a plasmid containing reverse complementary intron sequences flanking the circRNA sequence to promote backsplicing (**Fig. 6**). Long inverted flanking repeats are frequently used in vector constructions to promote backsplicing and generate circular transcripts. CircR is a highly efficient plasmid (400-5000x higher than endogenous levels) to overexpress circRNAs, which consists of three parts: two reverse complementary sequences (~ 800 bp), and the sequence for circRNA circulation which can be cloned in between complementary intron fragments (~200 bp) (Liu et al., 2018). Later on, minirc2 plasmid was created using reverse complementary ZKSCAN 1 introns with the circular RNA exons into the inverted BsmBI sites in the multiple cloning site of the widely used minirc vector (obtained from AddGene(#60648), Jeremy Wilusz' laboratory) with an easy construct and high efficiency (unpublished).

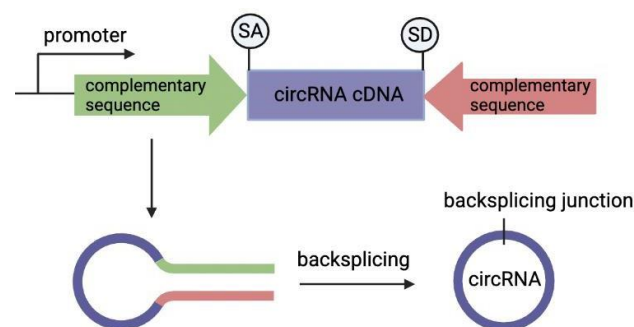


**Figure 6: Vector construction for overexpressing circRNAs.** Two Complementary sequences flanking the target circRNAs sequences promote circulation. The image was created by BioRender. (SA: splicing acceptor; SD: splicing donor).

## 1.6 Project basis

Many approaches are used to treat GBM, including surgery, radiotherapy, and chemotherapy. However, despite improvements in all of these areas over the past 30 years, the survival rate of GBM patients remains incredibly low. Tumour resistance to the frontline chemotherapy, TMZ, is another problem that GBM patients face (ANNOVAZZI et al., 2015). CircRNAs can not only regulate GBM cell proliferation, apoptosis, and invasion but also drug resistance (Zhu and Liu, 2019). Therefore, circRNAs offer a new way of thinking about the diagnosis and treatment of GBM. It is worth exploring more circRNAs that are related to GBM, which has the potential to improve survival from this malignant disease.

From high-throughput circular RNA sequencing of clinical glioma (grades II, III, and IV) and matched normal tissue samples, it was possible to identify circRNAs which are differentially expressed in disease (**Table 1**) (Conn et al., 2020). The hypothesis of this project is that regulating the expression of circRNAs can affect the oncogenic characteristics of GBM cell lines.

**Table 1: RNAseq Data Information.** Reproduced with permission from (Conn et al., 2020)

Sample Name	SANTB ID	Tumour Type	Grade	# Input reads	# Uniquely mapped reads
grade2_1	158	Astrocytoma	II	26,343,021	89.1%
grade2_2	190	Oligodendroglioma	II	27,302,075	88.8%
grade2_3	217	Oligodendroglioma	II	25,241,413	84.9%
grade2_4	207	Diffuse glioma	II	23,492,240	88.4%
grade2_5	267	Oligodendroglioma	II	15,437,385	39.1%
grade3_1	150	Anaplastic astrocytoma	III	21,617,416	86.6%
grade3_2	154	Anaplastic oligodendroglioma	III	29,164,440	90.8%
grade3_3	172	Anaplastic oligodendroglioma	III	42,012,355	66.5%
grade3_4	213	Anaplastic astrocytoma	III	25,758,766	87.6%
grade3_5	214	Anaplastic astrocytoma	III	28,412,184	85.7%
grade4_1	169	Glioblastoma	IV	28,268,617	87.6%
grade4_2	170	Glioblastoma	IV	27,580,126	82.7%
grade4_3	203	Glioblastoma	IV	27,106,465	88.4%
grade4_4	61	Glioblastoma	IV	29,197,512	83.0%
grade4_5	160	Glioblastoma	IV	23,140,292	86.4%
healthy_1	179	Control		22,852,102	80.3%
healthy_2	61_MC_NOR	Matched Control		29,806,403	87.3%
healthy_3	158_MC_NOR	Matched Control		28,019,827	88.2%
healthy_4	170_MC_NOR	Matched Control		26,038,920	89.1%
healthy_5	267_MC_NOR	Matched Control		24,372,321	73.3%

### 1.6.1 Project hypothesis

Overexpressing circRNAs which are lowly abundant in GBM tumours will affect GBM cell phenotypes.

### 1.6.1 Project aims

The aims of this project are:

1. Identify candidate circRNAs which are downregulated in GBM tumours compared with control healthy brain tissue
2. Generate GBM cell lines stably overexpressing candidate circRNAs
3. Assess phenotypes in circRNA overexpressing GBM cell lines

## 2. Materials and Methods

## 2.1 Analyses of RNA sequencing Data

### 2.1.1. Estimation of differential expression

High throughput RNA sequencing (RNAseq) was performed by Professor Simon Conn's lab on 20 brain samples donated to the South Australian Neurological Tumour Bank by consenting patients to identify circular RNAs (Conn et al., 2020). In this library, 82,049 circRNAs were identified across all samples, with a minimum of 2 reads in one sample. Differential expression analysis of RNAseq data was performed with average reads and a fold change of each circRNA between GBM and healthy brain tissue samples. CircRNAs with an average normalised read count  $\geq 10$ , and fold change  $> 3$  between two tissues were considered expressed differently. CircRNAs and mRNAs were mapped to the hg38 (Genome Reference Consortium Human Build 38).

### 2.1.2 Primer design

Primer 3 (Koressaar and Remm, 2007, Untergasser et al., 2012) was used to design primers for circRNAs, and premier biosoft NetPrimer was used to verify and visualise the quality of the primers. Acceptable primers were ones with undetectable, or very minor self-dimer, hairpin and cross dimer. The PCR product size range was 80-300bp, and the melting temperature ( $T_m$ ) ranged from  $56^\circ\text{C} - 58^\circ\text{C}$ . The position and orientation of the primers were visualised using the genome browser software, IGV (Broad Institute). The designed primers used for various experiments throughout the project are shown in **Table 2**.

**Table 2: Oligonucleotide primers used in this project.** For linear RNA targets, the exon location of the forward and reverse primers are shown in parentheses.

Targets	Primers (5'- 3')
<i>circMARK4(3,4)</i>	F: TCCGAGAAGTCCGCATCAT
	R: CAGGCTGCTGGGATTCAG
<i>mMARK4 (exons 12,13)</i>	F: AGTTCCTCTTCCACCTACCAC
	R: CTGCCTTGTTGGGGTTGT

<i>circGLIS3(2)</i>	F: AAGCCAAAGCAGCAGGAG
	R: TTTCAGGCAAAGTCCAATAAGT
<i>mGLIS3 (exons 9,10)</i>	F: GTGTGGTGCCTTCGTTTGA
	R: GCTTTTAGCCTTCGGTGTAGA
<i>circPTPN13(22-25)</i>	F: TCAGAATGCCCAAGGTCAA
	R: CCAGGCTTAGGAGGTGATGA
<i>mPTPN13 (exons 44,45)</i>	F: GACACGGAATGGTTCAGACA
	R: TTATTTTGGATAGAGAGCAGGAG
<i>circUSP25(2,3)</i>	F: GCTTTCCTTACTGCGAAGAAT
	R: CGTCTGCTGGTGTGTATCTG
<i>mUSP25 (exon 23)</i>	F: AATGAGCAAGCCGCAGAA
	R: CCAAGGTAGGAACACCATCG
<i>circZBTB20(4)</i>	F: TCACCGCCAAACAGAACTAC
	R: TGAAGGTTGATGCTGTGAATG
<i>mZBTB20 (exons 11-12)</i>	F: CTTTCACCGCCAAACAGAAC
	R: CACTGGTATGCCCTCACTCC
<i>circGLIS2(3,4)</i>	F: CTGCCTCCAGTGCCCAGT
	R: TCCTCTCCCGCTTCTCTCTT
<i>mGLIS2 (exons 7-8)</i>	F: CGCCTGGAGAACCTGAAGA
	R: TGCTCGTGGGACACAAAGT
<i>circEPHB4(11,12)</i>	F: CTCACAGAGTTCATGGAGAACG
	R: AAATTCCTCACAGCCTCATT
<i>mEPHB4 (exons 15,16)</i>	F: GCCATTGAACAGGACTACCG
	R: AACTTTCTTCGTATCTTCCCATTT
<i>circVCAN(3)</i>	F: ACAGATTCCTGATTGGCATT
	R: CTGTTTCTTCACTACAAGGTTTCATC

<i>mVCAN</i> (exons 12,13)	F: TGCTTAGGAAATGGAAGATGG
	R: GGAAAGGCACAGGAAGTTAGG
<i>circNFASC</i> (26,27)	F: TACACGTTGCGGGTTTATTC
	R: TTGTGCTTCCAGGTGATGTT
<i>mNFASC</i> (exons 29-30)	F: CCAAGGAAGAGGATGGCTCA
	R: CTGGGTGGGCTCCGTTAG
<i>circERC2</i> (13,14)	F: CGGATTGAGAGGAGGAAACA
	R: TTGATTGTGCTTGAGGTTGG
<i>mERC2</i> (exons 15-16)	F: AAGCAGCAGACCCAGAACAG
	R: ATGGTGGTGGTGGTGGTAAT
<i>circMLIP</i> (8-11)	F: TGGAAGATAACAGCGACCTCT
	R: TTCAGTCTTGGCTGGTTCATC
<i>mMLIP</i> (exons 12-13)	F: CCAATGGTGGCTATTCCTGA
	R: AAATCTCTTCTATGCTGGCTGTT
<i>circPPP1R13B</i> (2-4)	F: AGACCCAAGAGCAACGAACT
	R: CAGGTTGTTTCCGGTGTTATAG
<i>mPPP1R13B</i> (exons 15-16)	F: CATCCAGTGCTCCCAGTTTC
	R: TCAGTCTCGCTTTCGTCCTT
<i>circERC1</i> (14,15)	F: CCTGAAGCGGGAGAAGGA
	R: AGAGACTGCTGGGTGGAGG
<i>mERC1</i> (exons 16-19)	F: CTTCAAATCCTCCCATTC
	R: ATTGTCCCCTCACCTTTCTC
<i>circKCNN2</i> (8)	F: TGCCCAGGAACTGTACTCTTG
	R: TCTCCAGTCATCTGCTCCATT
<i>mKCNN2</i> , all isoforms (exons 12-13)	F: AACACTTTGGTGGACTTGGC
	R: CCTGATGGTCTGGCTTATGAG

<i>mKCNN2</i> , Isoform 1, 2 (exons 6-7)	F: ATGTTTCGGCATCGTGGTC
	R: TGTATTTCCCTGGCGTGGTA
<i>mKCNN2</i> , Isoform 1 (exons 7-8)	F: GCCAGGGAAATACAGTTGTT
	R: GGGATGAATAGCACACACCA
<i>mKCNN2</i> , Isoform 2 (exons 7-10)	F: ATACAGGTACCATGATCAACAGG
	R: CCAGCACCCATAATTCCAGT
<i>mKCNN2</i> , Isoform 3 (exons 1-2)	F: TGAGACCAAGAACCCACCA
	R: AACCACATCGCTCCAAGG
mini circ2 plasmid	F (BWS335): CTCGGATCCATAGTCCAGT
	R (BWS337): GATGGCTGGCAACTAGAAGG
<i>TBP</i> (exon 2)	F: CAGGCAACACAGGGAACC
	R: GGGAGGGATACAGTGGAGTG
<i>MALAT1</i> (exon 3)	F: GTCATAACCAGCCTGGCAGT
	R: GCTTATTCCCAATGGAGGT
<i>GAPDH</i> (exon 8)	F: CAGTGAGCTTCCCGTTCAG
	R: ACCCAGAAGACTGTGGATGG

## 2.2 Cell culture

### 2.1.1 Cell culture reagents

**Table 3: Reagents used for cell culture**

Reagent	Supplier	Catalogue number
---------	----------	------------------

Dulbecco's Modified Eagle Medium (DMEM) with 4.5 g/L D-Glucose, L-Glutamine and 110 mg/L Sodium Pyruvate	ThermoFisher Scientific	11995-065
Foetal Bovine Serum (FBS)	Bovogen	SFBS
Antibiotic-Antimycotic (100x)	ThermoFisher Scientific	15240-062
Phosphate Buffered Saline (PBS), pH 7.4 (10X) without Calcium Chloride and Magnesium Chloride	Gibco	70011-044
TrypLe without Phenol Red	Gibco	12604-021

### 2.1.2 Cell Lines

**Table 4: Cell lines used in cell culture experiments and the media used for their maintenance**

Cell Line	Origins	Media
U251	A 75 y, male with astrocytoma	DMEM + 10% FBS + 1% Anti-Anti (100X)
U87	A male with Glioblastoma	DMEM + 10% FBS + 1% Anti-Anti (100X)
HEK293	Human embryonic kidney cells	DMEM + 10% FBS + 1% Anti-Anti (100X)

### 2.2.1 Cell culture and passage

Cell lines U87 and U251 were grown in full media consisting of DMEM containing 10% FBS and 1% Antibiotic-Antimycotic. Cells were maintained at 37°C, 5% CO<sub>2</sub> and 95% humidity in 25 cm<sup>2</sup> cell culture flasks. When the confluency reached around 80%, cells were transferred to new flasks with fresh media. Briefly, media was aspirated, and cells were detached using TrypLE for 1 minute, followed by neutralisation with full media. Detached

cells were then transferred to new flasks containing full media with a maximum seeding dilution of 1:10. To enumerate cell numbers, 10  $\mu$ l detached cells were added to the CellDrop BF Brightfield Automated Cell Counter with an equal volume of trypan blue and counting of viable cells was used. Cell culture and all cell assays were performed in a class II biosafety cabinet under aseptic conditions.

### 2.2.2 Freezing/ thawing cells

Cells were cryopreserved in freezing media (50% FBS, 40% full media and 10% DMSO), with each cryovial containing  $\sim 1 \times 10^7$  cells in 0.5 ml freezing media. The vials were placed into a CoolCell® LX, at -80 °C for short-term storage, and in liquid nitrogen for long-term storage.

To thaw out cells, vials were rapidly defrosted in a 37 °C water bath just until the ice has disappeared, and all cells were transferred to a tube containing 5 ml full media, then centrifuged at 300 g for 5 minutes. The supernatant was removed and the pellet gently resuspended in 5 ml fresh complete medium and seeded into a 25 cm<sup>2</sup> flask.

### 2.3. RNA purification.

RNA was extracted from cells resuspended in TRIzol (ThermoFisher Scientific) using an RNA purification kit (ZymoPrep RNA mini kit) according to its protocol with on-column DNase digestion to remove genomic DNA. RNA concentration and purity were assessed using an Implen NP80 nano spectrophotometer. When A260/A280 & A260/A230 ratios were > 1.8, RNA was considered to have high purity, and was used for qRT-PCR.

### 2.4 Ribonuclease R (RNase R) treatment and purification

One microgram of RNA was digested by 0.2  $\mu$ l (4U) Ribonuclease R (Lucigen) with 3  $\mu$ l 10X RNase Buffer (Lucigen) and water up to 30  $\mu$ l. For checking RNase R treatment efficiency, a mock treatment group was set up with water instead of RNase R, and other

reagents were added in the same amount. Tubes were incubated at 37 °C for 30 mins (Eppendorf, ThermoTop). Following RNase R digestion, all samples were purified through a RNeasy®MinElute® Cleanup Kit (QIAGEN) according to the manufacturer's instructions.

## 2.5 Complementary DNA (cDNA) synthesis

Complementary DNA (cDNA) was synthesized from 750 ng of purified RNA using the Quantitect Reverse Transcription kit (Qiagen) according to the manufacturer's protocol. The whole process was performed on ice in a PCR-clean laminar flow. The final volume of 20 µl was diluted to 100 µl by the addition of 80 µl RNase-free water for RT-PCR and qRT-PCR.

## 2.6 Polymerase chain reaction (PCR)

PCR was set up with 10 µl 2X MyTaq HotStart Red mix, 1 µl 10 µM forward and reverse oligonucleotide primers, 2 µl diluted cDNA (1:5 diluted with RNase-free water) and 6 µl RNase-free water. Standard PCR cycling conditions used were initial activation of hotstart polymerase (95°C for 30 seconds) followed by 35-45 cycles of denaturing (95°C for 15s), annealing the primers (55°C for 15s) and extension (72°C, 5s). A final extension of 72°C for 1min was performed to fill in of incomplete DNA amplicons. Annealing temperatures were adjusted according to the melting temperature ( $T_m$ ) of primers, with gradient PCR performed to optimise annealing temperatures for qRT-PCR.

## 2.7 Agarose Gel Electrophoresis and Gel extraction

PCR products were separated by agarose gel electrophoresis for 40 mins at 90 volts using a Bio-Rad PowerPac Basic power supply. The agarose gel consisted of 1.8% Agarose in 1X TAE buffer with 1 µl of SYBR-safe DNA gel stain. The gel was loaded with 2 µl of 100 bp DNA ladder (New England Biolabs) and 20 µl of samples (PCR master mix contains loading dye). Gel products were imaged under UV and images were captured using an eBOX CX5 Gel imager (Vilber Lourmat). Bands corresponding to the correct size were excised from the gel and purified by the gel extraction kit (Qiagen).

## 2.8 Sanger sequencing

The sequence of purified PCR products, or plasmid DNA was analysed by Sanger sequencing (SALHN core facility).

## 2.9 Quantitative real-time RT-PCR

QRT-PCR was performed using 5 µl 2X Quantitect SYBR Green PCR Kit (Qiagen), 0.5 µl 10 µM forward and reverse primers, 2 µl diluted cDNA (1:5 diluted with RNase-free water) and water up to 10 µl. Three technical replicates and 1 non-template control (NTC) were performed for each reaction by using the Roter-Gene Q (QIAGEN). Cycling conditions were 95°C 10 minutes, followed by 40-50 cycles of 95°C for 15 s, 55°C for 15 s and 72°C 15 s. To compare transcript abundance, standard curves for each target encompassing six, ten-fold serial dilutions from  $4 \times 10^7$  to 40 copies using purified and quantified PCR products as the template. Amplification efficiencies and copy numbers were obtained from these graphs.

## 2.10 Transfection of cell lines

### 2.10.1 Plasmid extraction and digestion

Circular RNA overexpression was achieved using an overexpression plasmid developed in our laboratory, minirc2. This was a modification of the widely used minirc vector (obtained from AddGene (#60648), Jeremy Wilusz' laboratory) by removing the multiple cloning site to ensure the backsplice junction produced was as expected and to have higher circularisation efficiency. The plasmid's map is shown in **Fig. 7**.

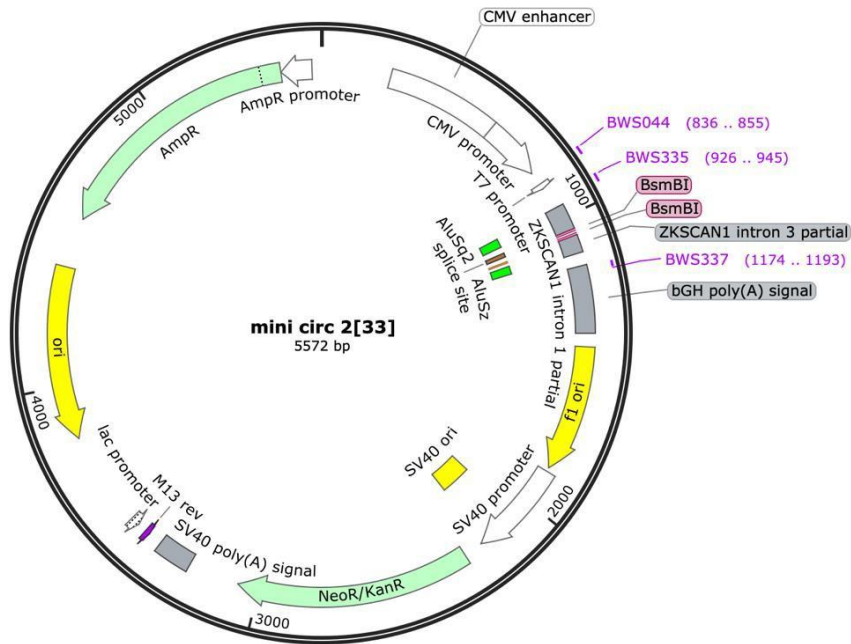


**Figure 7: Circular RNA overexpression plasmid.** Using reverse complementary ZKSCAN 1 introns with the circular RNA exons cloned into the inverted *BsmBI* sites in the multiple cloning site. Unpublished.

Plasmid-containing bacteria were grown in a 10 cm plate containing LB agar and ampicillin (100 µg/ml) and incubated at 37 °C overnight. A single colony was transferred to 2 mls of LB ampicillin broth and cultivated in a shaking incubator (37 °C, 200 rpm) overnight. Following this, plasmids were purified using the Isolate II plasmid miniprep kit (BioLine) according to manufacturers' instructions. One microgram of plasmids was then digested by 10 units of *BsmBI* (New England Biolabs) at 55 °C for 1h, to linearise for Gibson assembly.

### 2.10.2 Cloning and bacterial transformation

Fragments containing the exons of *circNFASC(26,27)*, *circPPP1R13B(2-4)* and *circKCNN2(8)* were designed to contain 25nt of flanking sequence homologous to the minicirc2 plasmid and ordered as synthetic DNA fragments (gBlocks, Integrated DNA Technologies), all these constructs were shown in Appendix I. These were cloned into the minicirc2 vector, which was linearised by digestion with *BsmBI* and agarose gel purification, by Gibson assembly using NEBuilder HiFi DNA Assembly Master Mix (New England Biolabs) (New England

Biolabs) according to Manufacturer's instructions. Three circRNAs (*circPPP1R13B(2-4)*, *circNFASC (26,27)* and *circKCNN2(8)*) fragments were cloned (the molar ratio of insert fragments to plasmid is 3:1) and then transformed into chemically competent TOP10 *E. coli* based on Chemically Competent Cells Transformation Protocol (New England Biolabs).

#### 2.10.4 Screening bacterial colonies

Ten individual colonies from each plate were transferred to 20µl LB broth, which was used as the PCR template. PCR was set up with 12.5µl 2X MyTaq HotStart Red mix, 1 µl 10 µM BSW335 and BSW337, 1 µl colony suspension and water up to 25µl. BSW335 and BSW337 are two convergent primers that flank the cloning site in the mini circ2 plasmid. PCR products were separated by agarose gel electrophoresis, 1X TAE buffer containing 1% agarose. The colonies with the correct size amplicon were cultured overnight and purified plasmids were submitted for Sanger sequencing.

#### 2.10.5 Transient transfection

In order to verify the plasmids produced the correct product, U251, U87 and HEK293 were transiently transfected with the circRNA overexpression plasmids. Cells were inoculated into 12-well plates at a confluency level that would reach 70% - 90% on the day of transfection. Plasmid (500ng) was mixed with OptiMEM reduced serum media (50ul) and 1.5 µl Lipofectamine 2000 transfection reagent (Invitrogen) was mixed with 50ul Opti-MEM. These were mixed, briefly vortexed and incubated at room temperature for 5mins. This mixture was gently added dropwise to the culture medium and cells were incubated for 24-48 hours.

#### 2.10.6 Gradient PCR

Gradient PCRs were set up with 5µl 2xSYBR Green, 0.5µl 10µM forward and reverse primers, and 4µl diluted cDNA (1:5 diluted with RNase-free water). For getting optimal annealing temperature, the annealing temperatures were set from 53°C to 57°C (57°C; 56.5°C; 55.9°C; 54.9°C; 53.8°C and 53°C) by using BIO-RAD CFX Opus 384 Real-Time PCR System.

### 2.10.7 Nuclear:cytoplasmic fractionation

When cells reached ~80% confluence in 75 cm<sup>2</sup> flask, media was aspirated and cells were washed with PBS once and trypsinised using 1 ml, TrypLE for 2 minutes in a 37 °C incubator. For neutralizing TrypLE, 9 ml fresh media was added. Cells were washed off the flask by pipetting the media down the bottom of the flask 3 times. Around 0.5 ml cells were used for counting, and the left cells were centrifuged at 300 g for 5 minutes at room temperature. Cells were counted by mixing cells and Trypan Blue Stain (0.4%, Gibco; lot: 1184780) at a ratio 1:1, and then 10 µl of the mixture was loaded to Brightfield Cell Counter (DeNovix) using Trypan Blue mode for counting viable cells. After centrifugation, the supernatant was removed, the cell pellet was resuspended in the desired amount of fresh media, and ~2.5x10<sup>6</sup> cells were collected for cell fractionation. These cells were then washed with 10 ml of PBS twice, and the pellet was immediately kept on the ice for cell fractionation based on the PARIS kit manufacturer's instruction.

An equal amount of cytosolic and nucleus fractions was used for the synthesis of cDNA followed by qRT-PCR for checking the localization of circRNAs. *MALAT1* and *GAPDH* were used as nucleus and cytoplasm controls respectively. *MALAT1* is an abundant non-coding RNA highly enriched in the nucleus, which can be used as nuclear control, while *GAPDH* is an mRNA highly enriched in the cytoplasm, which can be used as cytosolic control.

### 2.10.8 Transfection U251 and U87 cell lines

U251 and U87 cells were split into a 6-well plate at 25-30% confluence. After 24h, confluence reached 50% - 60%, and two micrograms of plasmid DNA were transfected into cells using 7.5 µl Lipofectamine 2000 transfection reagent (Invitrogen) following the Lipofectamine<sup>®</sup> 2000 DNA Transfection Reagent Protocol.

Neomycin (G-418) selection was applied after cultivation for 48h. G-418 solution (Roche, ref: 0472 7878 001) at 600 µg/ml was slowly added to the media, which has been previously determined by Dr Brett Stringer that this is the optimal concentration for selecting U251 and U87 cells with mini-circ2 plasmid. Half of the media was changed after 3 days. On day 7, transfected cell lines were established.

## 2.11 Cell assays

### 2.11.1 Cell growth rate analysis

Viable cells were counted following trypsinisation and neutralization from 75 cm<sup>2</sup> flasks and resuspended at 1 x 10<sup>4</sup> cells/ml in complete media containing G-418 and 1:1000 dilution of IncuCyte NucLight Red (lot:19N213-060721). Two thousand cells (in 200 µl media) were plated into a clear, flat-bottomed 96-well cell culture plate (Corning Incorporated; REF: 3599) with 6 technical replicates. The selected wells were imaged using the IncuCyte SX5 instrument (Essen Bioscience) every 2 hours for 5 days collection of brightfield and red fluorescent channels.

### 2.11.2 Cell size and shape analysis

Cell size and shape analysis was conducted by Operetta CLS High Content Analysis System after fixing cells using 4% paraformaldehyde (PFA; ProSciTech; lot:220714-50) and staining cells using the following reagents: CellTracker Deep Red (C34565, 1:1000) and PhalloidiniFluor488 (ab176753, 1:1000)). Briefly, 1,000 cells in 100 µl full media with G418 solution were plated in black 384-well plates with flat, clear bases with 6 technical replicates and cultivated overnight. Cells were fixed in 4% PFA in PBS for 10 minutes at room temperature followed by three PBS washes. To stain cells, 50 µl PBS containing stain reagents was used for 1h at room temperature in the dark. Before imaging with CLS, cells were stained with 0.1 µg/ml DAPI (4',6-diamidino-2-phenylindole) for 10 mins to visualise nuclei and then washed once with PBS.

### 2.11.3 Colony Formation Assay

A colony formation (soft agar) assay was set up to measure the ability of cells to form colonies as an in vitro assessment of the tumourigenicity. The assay was conducted in 24-well plates with 6 technical replicates. Each well had three layers: the bottom layer, the top layer and the feeder layer. The bottom contains 4% low-melting point agarose (12%), DMEM with 10% FBS (70%), additional FBS(13%) and sterile deionised water (5%). After heating all the reagents to 42 °C, they were mixed by pipetting up and down and then quickly plated out 500 µl to each well. After around 30 mins, the bottom layer was solidified. The top layer was set up with 1,300 cells in 350 µl complete media, along with 4% low-melting point agarose (8.6%), additional FBS (13%) and sterile deionised water (8.4%). All the reagents were kept at 42 °C except for the cell suspension, which was in a 37 °C incubator. When the top layer solidified, 100 µl complete media (Feeder layer) was added to each well to avoid gel evaporation. Care was taken to ensure no bubbles formed in either layer. The component of each layer has been shown in **Fig. 8**. The plate was then incubated for 14 days and then was imaged using a GelCount imager (Oxford Optronix) on Day 14.

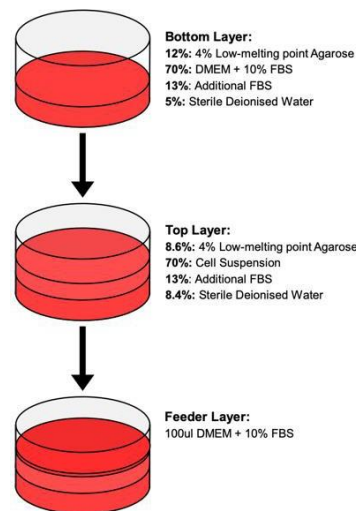


**Figure 8: Soft Agar reagents in each layer.** A 4% low-melting point agarose (LM agarose) solution was obtained by autoclaving a mixture of UltraPure™ Low Melting Point Agarose (Invitrogen) and sterilized water for 20 mins at 121°C and 15 psi. LM agarose is the component for forming a gel in the bottom and top layers, and the gel can be solidified in around 30 mins at 24 to 28°C sitting in a class II biosafety cabinet. All the reagents must be pre-heated up to 42°C before mixing except for the cell suspension, which was kept at 37°C. Each well had approximately 1300 cells.

## 2.12 Protein analysis

**Table 5: RIPA Buffer for protein extraction**

<b>Reagent</b>	<b>Volume per 100 ml of solution (v/v)</b>	<b>Final concentration</b>
Sodium Chloride (NaCl) (1M)	15 ml	150 mM
Nonidat P-40 (1%)	1 ml	1%
Sodium deoxycholate (DOC) (10%)	5 ml	0.5%
Sodium Dodecyl Sulfate (SDS) (10%)	1 ml	0.1%
Tris (2 M, PH: 7.4)	2.5 ml	50 mM
ddH <sub>2</sub> O	75.5 ml	

### 2.12.1 Protein extraction

Pelleted cell samples (~ 2.5 million cells) were thawed on ice. Once thawed, cells were lysed using 250  $\mu$ l RIPA Buffer containing 25  $\mu$ l protease inhibitor stock solution, which was made by dissolving one tablet protease inhibitor (cOmplete Tablets, Mini EDTA-free, EASYpack; Roche, Basel, Switzerland; lot: 32995700) by 1 ml RIPA Buffer. The lysate was maintained under constant agitation for 30 mins at 4 °C, and then was centrifugated for 16,000 g for 20 mins at 4 °C. Supernatant containing proteins was carefully transferred to an ice cold 1.5 mL Eppendorf tube.

### 2.12.2 Bradford protein quantification assay

Bradford assay was used to quantify protein concentration in cell lysates. A standard curve was made by setting up 6 different concentrations (2 mg/ml, 1 mg/ml, 0.5 mg/ml, 0.25 mg/ml, 0.125 mg/ml and 0.0625 mg/ml) of Bovine Serum Albumin (BSA) in technical triplicates. Protein samples were diluted using water at a ratio of 1 in 10 with three technical replicates. After adding protein stain (BIO-RAD Bradford assay reagent, catalogue: 500-0006) for incubating 5 minutes at room temperature, the plate was read by CLARIOstar Plate Reader (BMG LABTECH) at 595 nm.

### 2.12.3 Western blotting

Protein lysates (20 µg) premixed with 5X SDS loading dye (10% SDS; 30% Glycerol; 250 mM, 0.5 M Tris-Cl (PH: 6.8); 5% Beta-Mercaptoethanol; 0.9% Bromophenol blue) were heated for 5 mins at 95 °C and then separated by loading them onto a precast gel along with 5 µl Precision Plus Protein™ Kaleidoscope™ Prestained protein standards (BIO-RAD, catalogue number: #161-0375) onto precast Any kD Mini-PROTEAN TGX Stain-Free Gels (BIO-RAD; catalogue number #4568124) based on the manufacturer's instructions. The proteins were electrophoresed at 200V for 40mins. After electrophoresis, the gel was imaged using the stain-free protocol on the BioRAD imager Gito for activating for 1 minute to determine total protein loading, used for normalising between lanes.

Proteins were transferred onto a Nitrocellulose membrane (BIO-RAD, 0.2 µm; lot: # 1620112) by the wet transfer protocol in transfer buffer (25 mM Tris, 190 mM Glycine, 20% Methanol) at 80V for 50 minutes at 4 °C. Care was taken to make sure to remove bubbles from the gel-membrane-filter paper sandwich. Protein transfer was visually confirmed by observing the transfer to the prestained protein ladder.

The membrane was then blocked in 5% skim milk powder in TBS (20 mM Tris, 150 mM NaCl) at room temperature for 1 hour. The primary antibody, rabbit anti-KCNN2 (SIGMA-ALDRICH, catalogue number: SAB2101228, lot: QC4717), was diluted 1:1000 in fresh blocking buffer (5% skim milk powder in TBS) and added to the membrane and gently rocked overnight at 4 °C. The next day, the blot was washed with TBS-T (TBS with 0.1% Tween 20) three times for 5 mins each wash, and then the second antibody (goat anti-rabbit-

HRP conjugate) at a dilution of 1:10,000 in 5% skim milk in TBS-T was applied for 1 hour at room temperature. Then, the membrane was again washed with TBS-T three times for 5 mins each wash.

The HRP signal was then developed by exposing the membrane to SuperSignal™ West Pico PLUS Chemiluminescent Substrate (ThermoFisher Scientific, catalog number: 34580) using an equal volume of Luminol/Enhancer Solution and Stable Peroxide solutions and incubated for 5 mins. The chemiluminescent signal was captured using the ChemiDoc XRS+ imaging system (BioRad). A colour image was collected to observe the prestained ladder bands on the same membrane to more accurately estimate the size of the band.

### **3. Results**

#### **3.1 Analysis of RNAseq Data for candidate selection**

##### **3.1.1. Estimated differential expression between GBM and non-tumour tissue**

High throughput RNA sequencing libraries for both circular RNA and mRNA-seq, separately, were analysed for 20 tissue samples. These samples included 15 primary gliomas, with five grade II, five grade III, and five grade IV (GBM) tumours and five healthy brain tissue samples (control tissues). In the control tissues, four tissues matched with primary glioma samples, meaning they were from the same patient, which included two matched with grade II gliomas and two matched with GBM tumours. This data underwent QC and was mapped to the hg38 human genome assembly by the bioinformatician, Dr. Shashikanth Marri. The circRNA-seq data has already been published and is publicly available at the Gene Expression Omnibus with accession number GSE159260 (Conn et al. 2020), while the mRNAseq data is presented here for the first time.

##### **3.1.2. Selection of circRNA candidates**

The purpose of this research project is to investigate circRNAs that are differently expressed between GBM cells and healthy brain tissues. Therefore, I focused on comparing the five

GBM tumours with five healthy brain tissue samples. Given the limited research time for this project, 14 differently expressed circRNAs were shortlisted based on the criteria of 0.07-67-fold changes of expression level between healthy brain tissues and GBM tumours. Eight of these were upregulated in GBM ranging from 3.6-10-fold increase (**Fig. 9A**), and six were downregulated in GBM with a 10-67-fold decrease (**Fig. 9B**). Meanwhile, their endogenous mRNA expression level was also analysed in the GBM mRNA-seq, with all parent mRNAs showing higher expression in GBM samples ranging from 1.1-6.9-fold increase (**Fig. 9C**). While among the six downregulated circRNAs in GBM, mNFASC, mPPP1R13B, mMLIP, and mERC2 are downregulated in GBM with a 1.4-4-fold decrease but no statistical significance, however, mERC1 and mKCNN2 are upregulated with a 1.9-fold and 1.3-fold increase respectively (**Fig. 9D**). Therefore, circERC1 (exons 14-15) and circKCNN2 (exon 8) were prioritised as there was an apparent misregulation compared to the parent mRNA. According to the preferred circRNA nomenclature – the name of the gene with exons of the circRNA in parentheses - these are referred to as *circERC1(14,15)* and *circKCNN2(8)*(Chen et al., 2023). Meanwhile, for ensuring candidate circRNAs have not been explored, their functions and their parent gene functions were researched (Appendix II). This approach was validated as two of the shortlisted circRNAs, *circGLIS3(2)* and *circEPHB4(11,12)*, have been demonstrated to be upregulated in GBM cell lines (Li and Lan, 2021, Jin et al., 2021). As a result, these were excluded from further investigation in this study.

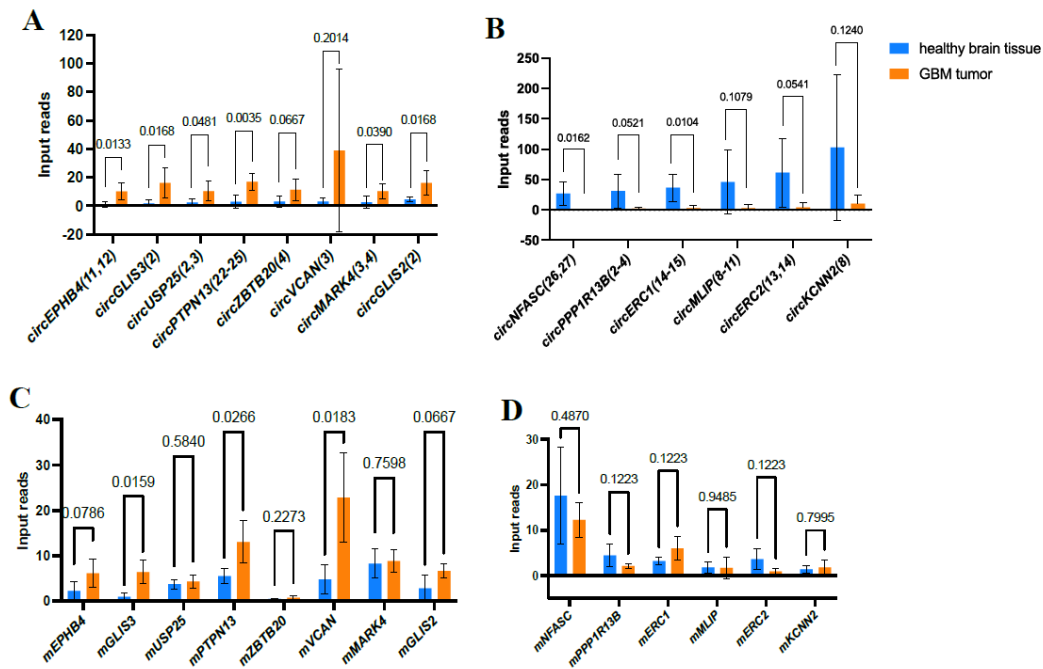


**Figure 9 : Expression levels of candidates circRNAs and their cognate mRNA in GBM**

**tumours versus healthy brain tissue.** A) Upregulated and B) downregulated circRNAs from healthy brain tissue to GBM tumour tissue using circRNA sequencing. C) Upregulated and D) downregulated candidate circRNAs endogenous mRNA expression level. Data are displayed as backsplice junction count (mean  $\pm$  standard deviation) (n=5). Statistical significance was determined by one-way ANOVA. The P-value is indicated above the paired columns.

### 3.2. Validation of primers for circRNA candidates

#### 3.2.1. PCR validation of circRNA Primers

RT-PCR was performed using primers designed against the 14 circRNA candidates (**Table 2**). Complementary DNA (cDNA) from the most commonly used, established GBM cell lines, U251 and U87, were used and primer annealing conditions were optimised using gradient PCR (temperatures ranging from 52-60 °C). Using the optimum conditions for each primer set, the PCR products were separated by agarose gel electrophoresis (**Fig. 10**). Of the eight upregulated circRNA candidates, four (*circGLIS3(2)*, *circPTPN13(22-25)*, *circZBTB20(4)* and *circEPHB4(11-12)*) were found to produce a single PCR product in both

cell lines. These would be ideal candidates to perform knockdown studies, however, due to time constraints this was not attempted. For the six downregulated circRNAs in GBM, none produced a single band in both cell lines. However, *circERC2(13-14)*, *circMLIP(8-11)* and *circPPP1R13B(2-4)* produced a single band in U251 cells, *circKCNN2(8)* produced a single band in U87, and *circNFASC(26-27)* was not amplified in either cell lines. For the circRNAs where multiple bands were detected across both cell lines, these were excluded from further study. All remaining circRNAs with strong bands at the expected size were sent for Sanger sequencing except for *circGLIS3(2)* and *circEPHB4(11-12)* which were not prioritised as these two circRNAs had already been validated as upregulated in GBM (Li and Lan, 2021, Jin et al., 2021).

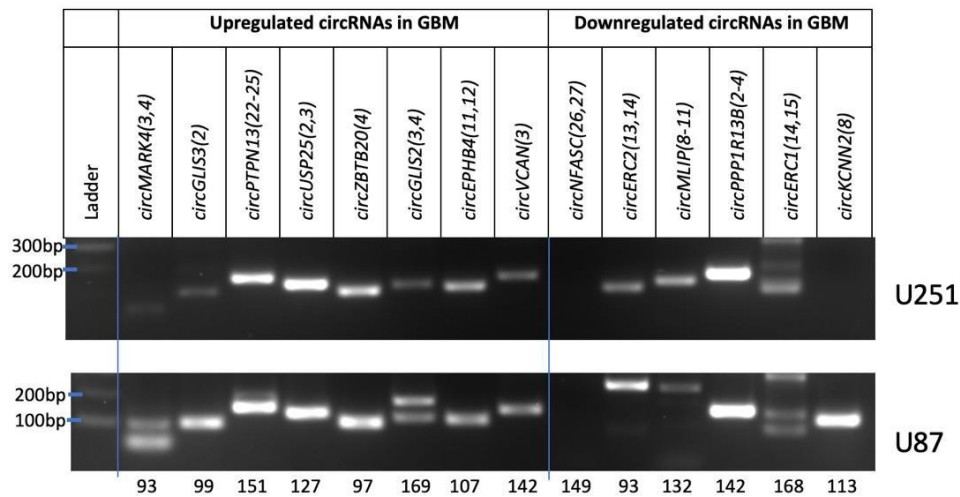


**Figure 10: Validation of circRNA primers and circRNAs expression in U251(upper) and U87 (lower) cell lines.** All expected product sizes are presented by numbers under each lane.

To amplify the parental mRNAs, mixed cDNA from both U251 and U87 cell lines was used and RT-PCR performed. The PCR products were separated by agarose gel electrophoresis, with single bands amplified for all targets (**Fig.11**). Interestingly, despite *circNFASC* not being amplified in either cell line, its mRNA was amplified.

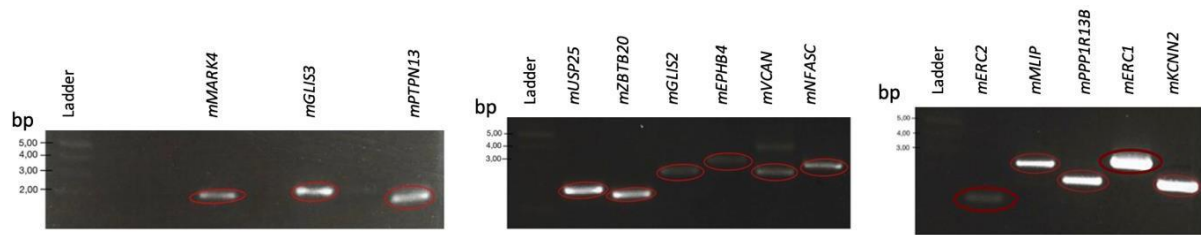


**Figure 11: RT-PCR of mRNAs from GBM cells (mixed U251 and U87).** Agarose gel electrophoresis of all products with expected sizes has been circled in red.

### 3.2.2. Sequencing of PCR products

PCR products for *circPTPN13*(22-25), *circUSP25*(2,3), *circZBTB20*(4), *circGLIS2*(3,4), *circERC2*(13,14), *circPPP1R13B*(2-4) and *circKCNN2*(8) were purified from the gel and then sent for Sanger sequencing. Except for *circGLIS2*(3,4), all circRNAs were confirmed to have the expected back splice junctions (**Fig.12**). Since there were two close bands in the *circGLIS2* (3,4) gel image, it is possible that the incorrect band was excised, but having an excess of suitable circRNA candidates to focus on, I did not proceed with further analysis of this target. Additionally, the RT-PCR products for the cognate mRNAs were also sent for Sanger sequencing. All products from the RT-PCR on mRNA sequences aligned perfectly with the expected sequence using BLASTn (Appendix III).

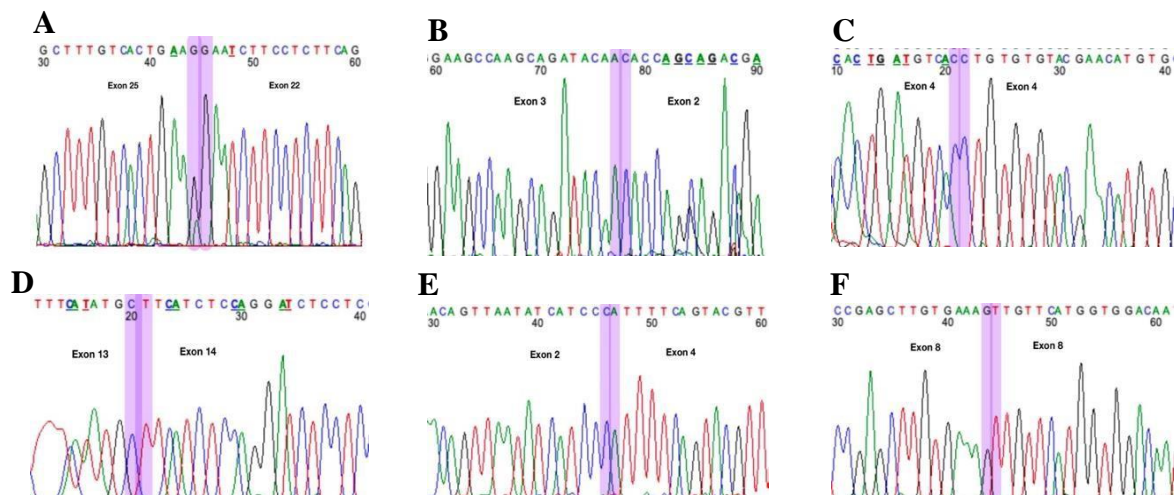


**Figure 12: Candidate circRNA Sanger sequencing chromatograms.** A) *circPTPN13*(22-25); B) *circUSP25*(2-3); C) *circZBTB20*(4); D) *circERC2*(13,14); E) *circPPP1R13B*(2-4); F) *circKCNN2*(8). The back splice junctions have been shown by highlighting the nucleotide on

either side in purple and listing the exons to which the sequence corresponds. Images were extracted using FinchTV (ver1.4.0) chromatogram viewer.

### 3.3 selection of circRNA candidates

I decided to focus on overexpressing circRNAs which were found to be downregulated in GBM as the method of overexpressing circRNAs has been well-established in our laboratory. I decided to choose three circRNAs and the criteria I used to select these were choosing a circRNA which was absent from both U87 and U251 cell lines (*circNFASC(26-27)*), one present in both cell lines (*circPPP1R13B(2-4)*) and one circRNA detected in only a single cell line (*circKCNN2(8)*) which was found in U87 and not U251 cells.

### 3.4 overexpressing circRNA candidates

Overexpressing circRNA candidates in U251 and U87 cell lines was achieved by transfecting the cells with a plasmid DNA construct encoding the specific circRNA. The plasmid is called mini circ2, designed by Dr. Brett Stringer, and is a modified version of a publicly available vector called pcDNA3.1(+) CircRNA Mini Vector (AddGene plasmid #60648) which uses inverted introns from the *ZKSCAN1* gene to promote circularisation of anything cloned into it. The mini circ2 vector improves on the original vector as it simplifies cloning, by replacing the multiple cloning site with inverted *BsmBI* sites (akin to Golden Gate cloning) which also ensures the correct circRNA is produced without any molecular scars remaining in the back splice junction. Once cloned and sequence-verified, the plasmids were transfected into U87 and U251 cells by lipofection, and selection with G418 in the culture media was undertaken for 7 days. A G418 kill curve was previously performed by Dr. Brett Stringer, and the concentration of G418 which would kill non-transfected cells in 7 days was 600 µg/ml for both U251 and U87 cells.

#### 3.4.1. Plasmid digestion

To clone the desired circRNA, minirc2 was digested using the restriction enzyme *BsmBI*, producing two fragments: 22 bp and 5550 bp. For visualizing and checking the digestion

efficiency, the digested plasmid underwent 1.2% agarose gel electrophoresis (**Fig. 13**) and the larger fragment was gel purified and used for cloning.

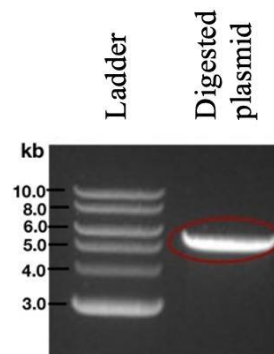


**Figure 13: Digest of mini circ2 plasmid with BsmBI.** A single, linear band was seen at the expected size, which has been circled in red.

#### 3.4.2. Gibson assembly and colony PCR

The exon sequences for the three circRNAs - *circPPP1R13B(2-4)*, *circKCNN2(8)* and *circNFASC(26-27)* - were synthesized as gene fragments and each contained 25 nt of vector homologous sequence on the ends to enable Gibson assembly into the *BsmBI*-digested minicirc2 plasmid. After transforming the chemically competent TOP10 *Escherichia coli* bacteria by heat shock, these were plated onto LB agar plates with ampicillin overnight. Ten single colonies underwent colony PCR with vector-specific primers (BWS335 and BWS337, which were provided by Dr Brett Stringer) flanking the cloning site to detect amplification of the inserted DNA fragments.

Colony PCR products then underwent 1% agarose gel electrophoresis (**Figure 14A, B**).

Based on the results, the ligation efficiency was 100%. The expected size for amplifying the exons cloned in for *circPPP1R13B(2-4)*, *circKCNN2(8)* and *circNFASC(26,27)* is 632 bp, 557 bp, and 706 bp respectively. Colony #8 for *circPPP1R13B(2-4)*, colony #1 for *circNFASC(26,27)*, and colony #4 for *circKCNN2(8)* were selected to do Sanger sequencing (**Figure 14 C-E**).

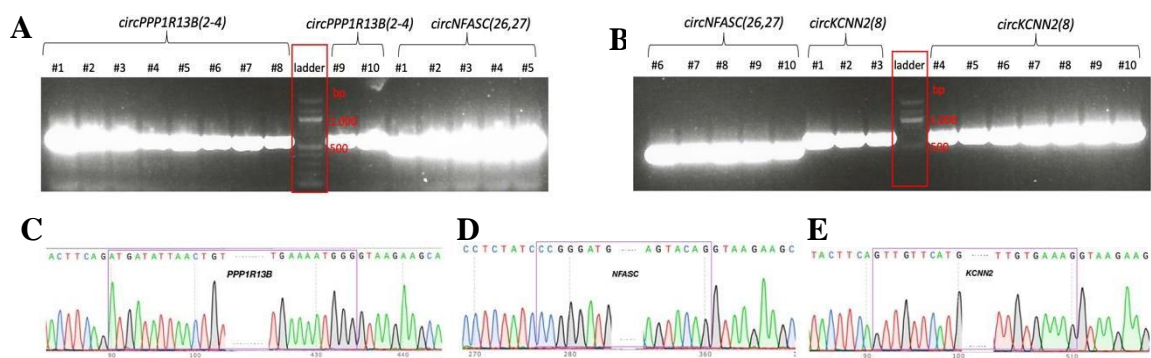


**Figure 14: Colony PCR results and sequence confirmation of circRNAs cloned into the minirc2 plasmid.** (A-B) Colony PCR to verify the presence of minirc2 plasmid containing target circRNAs. Ten colonies (#1-#10) were selected for each target circRNAs. The expected size of minirc2 containing *circPPP1R13B(2-4)*, *circNFASC(26,27)* and *circKCNN2(8)* is 632 bp, 557 bp, and 706 bp respectively. (C-E) Sequencing results to verify minirc2 plasmid containing target circRNA exons. The circRNA exons cloned into the vector are shown in purple boxes.

#### 3.4.4. Transient transfection

Both U251 and U87 cell lines were assessed after transfecting cells for 24 hours, and all of these overexpressions are statistically significant. In U251 cells, *circPPP1R13B(2-4)* expression level has been increased by 644 fold, and *circKCNN2(8)* and *circNFASC(26-27)* were detectable with 13,755 copies and 478,099 copies respectively after transient transfection by quantitative RT-PCR (**Fig. 15A**). In U87 cells, *circPPP1R13B(2-4)* expression level has been increased by 9,430 fold, *circKCNN2(8)* expression level has been increased by 1,511 fold, and *circNFASC(26,27)* can be detected with 3,334,267 copies after transient transfection (**Fig. 15B**). The results have been normalised by a housekeeping gene, TBP, and the standard curves for calculating circRNAs and TBP transcript abundance are in Appendix IV.

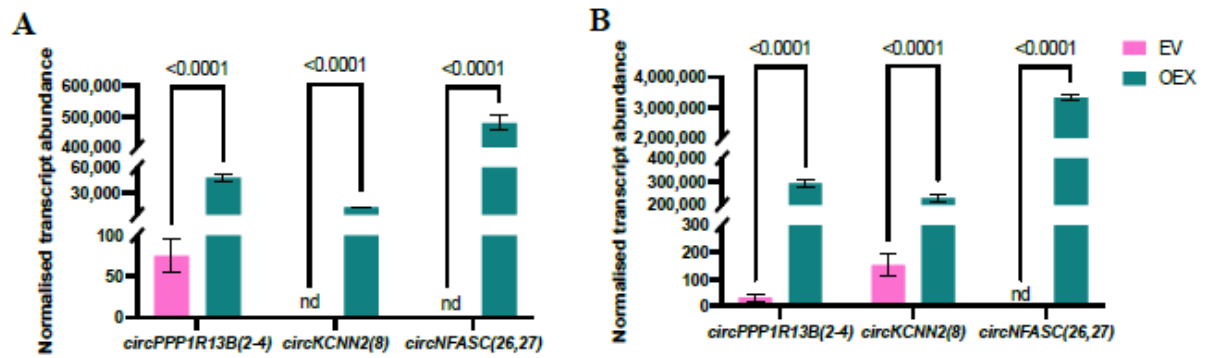


**Figure 15: qRT- PCR validation of target circRNAs overexpressed in U251(A) and U87(B) after transient transfection.** Data has been normalised based on the ratio of TBP copies between EV and OEX. Results were displayed as mean with standard deviation (N=3). Statistical significance was determined by multiple t-tests. ( $P$ -value  $< 0.05$ : statistically significant)

After running qRT-PCRs, I also confirmed all of these amplicons are the expected products by Sanger sequencing. If it was not correct, the result often shows cross-banding on the chromatogram after reaching the back splice junction. However, all products contained the correct circRNA with an accurate back splice junction only (**Fig. 16,17**).

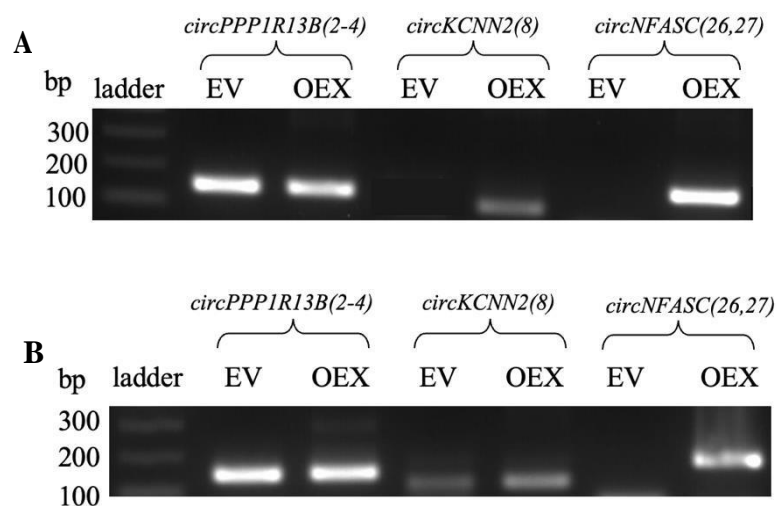


**Figure 16: Transient transfection products (A) U251 and (B)U87 separated by agarose gel electrophoresis.** The expected product size for *circPPP1R13B(2-4)* is 142 bp, for *circKCNN2(8)* is 113 bp, and for *circNFASC(26,27)* is 166 bp. Note: EV: empty vector (mini circ2 plasmid). OEX: overexpressing.

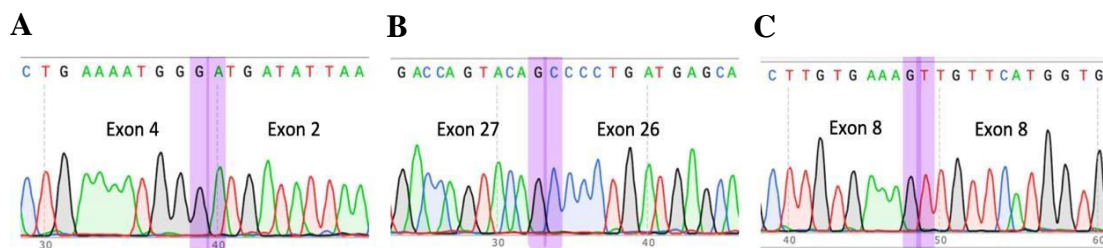


**Figure 17: Sanger sequencing results confirming transgenic circRNAs produce the correct back splice junctions in U87 overexpressing cell lines. A) *circPPP1R13B(2-4)*; B) *circNFASC(26,27)*; C) *circKCNN2(8)*. The back splice junctions have been highlighted in purple. The sequencing test was performed by SA Pathology Sequencing Facility Flinders using the method of Sanger Sequencing**

### 3.4.5 RNase R resistance of circRNA

To validate that the PCR amplicon is from a *bona fide* circRNA and not from a linear concatemer (where linear RNAs are ligated in the same order as you would see for a circRNA), digestion with an exonuclease, such as Ribonuclease R (RNase R), is required. RNase R digests single-stranded RNA from the 3' end of linear RNAs, including mRNAs and linear concatamers, while circRNAs and linear RNAs which form double-stranded RNA through base-pairing are resistant to degradation. To achieve this, RNA was purified from the U87 cell line and was treated with RNase R or via mock digestion (without RNase R). RT-PCR was performed for each of the three circRNA and in each case, the circRNA abundance was largely unaffected by looking at the intensity of the band from non-saturating PCR conditions. Regarding the mRNAs, two of the three mRNA products (*NFASC* and *KCNN2*) were unable to be amplified following RNase R digestion, while the mRNA for *PPP1R13B* seemed to partially resist the digestion as the band intensity was approximately 50% of the undigested control (**Fig. 18**).

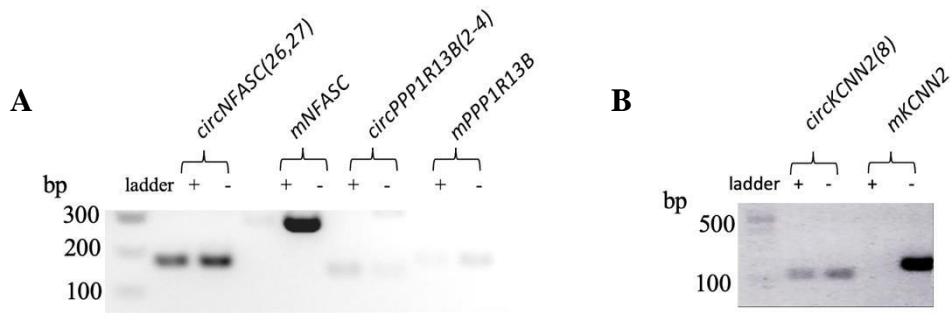


**Figure 18: RNase R digestion for validating circRNAs.** RNase R digestion products. **A)** *circNFASC(26,27)*, *mNFASC*, *circPPP1R13B(2-4)*, *mPPP1R13B*, and **B)** *circKCNN2(8)* and *mKCNN2* were visualized by gel electrophoresis. The expression level of *circNFASC(26,27)*, *circPPP1R13B(2-4)* and *circKCNN2(8)* were unaffected, while *mNFASC*, *mPPP1R13B* and *mKCNN2* expression was lost following RNase R treatment. (+: with RNase R treatment; -: without RNase R treatment).

#### 3.4.6 Stable CircRNA overexpression

Minicirc 2 plasmids containing *circPPP1R13B(2-4)*, *circNFASC(26-27)*, *circKCNN2(8)* or with no insert (empty vector) were used to transfect U251 and U87 cell lines to establish stable cell lines. Transfected cells were initially selected with 600  $\mu\text{g/ml}$  G-418 solution for 7 days. After seven days of selection, all untransfected cells had died, indicating that all attached surviving cells in the transfected groups were successfully transfected (**Fig. 19**).

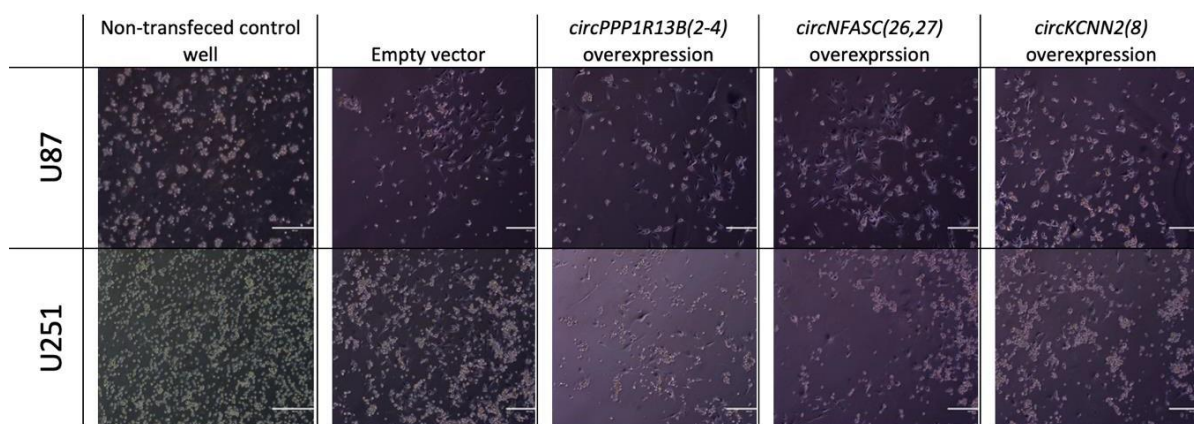


**Figure 19: Transfected GBM cells 7 days after initially G-418 solution selection compared to a non-transfected control well.** There were no live cells in the non-transfected control well, while live cells were in empty vector, *circPPP1R13B(2-4)* overexpression,

*circNFASC(26,27)* overexpression and *circKCNN2(8)* overexpression wells, indicating target circRNAs have been successfully transfected to U87 and U251 cells. Images were obtained by using Invitrogen EVOS XL with 10X magnification, and the scale bar was 400  $\mu$ m.

After transfected cell lines were established, RNA was harvested to assess the level of overexpression. Importantly, cells were harvested at no more than 80% confluence. In each case, the circRNA abundance was found to be statistically significantly increased (**Fig. 20**). Three biological replicates were conducted with overexpressing *circPPP1R13B(2-4)* in U251, and overexpressing *circKCNN2(8)*, *circNFASC(26,27)* in U87. A single biological replicate was performed by overexpressing *circKCNN2(8)* and *circNFASC(26,27)* in U251 cells, and overexpressing *circPPP1R13B(2-4)* in U87 cells since there were no phenotypic changes were observed after transfection.

Based on the results, all these three circRNAs have been overexpressed with different levels: *circPPP1R13B(2-4)* expression levels have been increased 4.2 fold in U251 and 5.9 fold in U87; *circKCNN2(8)* can be detected in U251 with 100 copies and increased the expression of 12.2 fold in U87; *circNFASC(26,27)* is detectable in both U251 and U87 cell with 1,834 copies and 18,491 copies respectively.

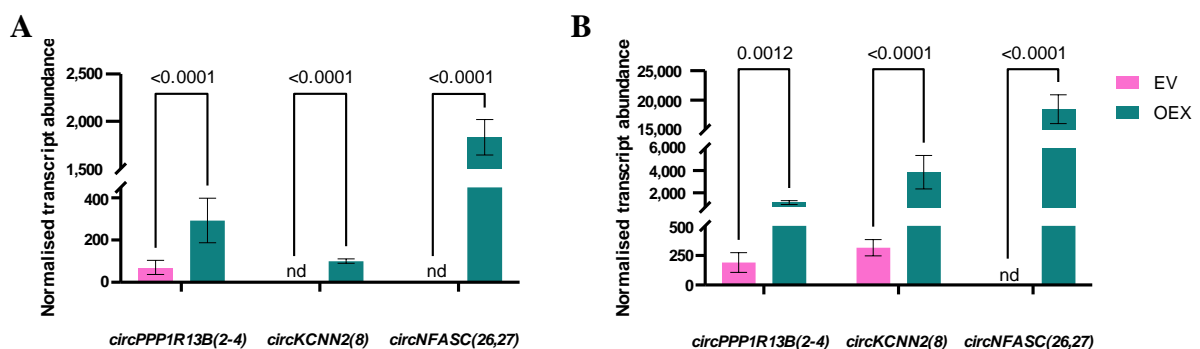


**Figure 20: Validation of target circRNAs expression level in (A) U251 and (B) U87 cells after transfection by qRT-PCR.** In U251 and U87 cells, the circRNA abundance was found to be statistically significantly increased. Data presented as mean  $\pm$  standard deviation (*circPPP1R13B(2-4)* in U251 and *circKCNN2(8)*, *circNFASC(26,27)* in U87: N=9; others: N=3). Data has been normalised based on the ratio of TBP copies between EV and OEX.

Statistical significance was determined by multiple t-tests, and the *P*-values are shown. ( *P*-value < 0.05: statistically significant; nd: non-detected).

As some circRNAs are known to impact the expression of their parent mRNA, after confirming their circRNA expression level, I also assessed their parent mRNA expression level in the first biological replicate of each generated line. While for five out of six lines, the parental mRNA did not change in its expression level, *mKCNN2* in U87 cells transfected with *circKCNN2(8)* showed a 5-fold increase (*P*-value <0.0001) (**Fig. 21B**). However, when I made another two biological replicates, this increase was no longer found (**Fig. 21C**).

All mRNA primers that were originally designed are sitting at the 3' end of genes for capturing the maximum number of potential splice variants of the RNA. For exploring which splice variants of *mKCNN2* were affected (including those incorporating the *circKCNN2(8)*) by overexpressing *circKCNN2(8)*, four more specific primer pairs were designed (**Fig. 21A**). Overexpressing *circKCNN2(8)*, 47 fold above empty vector, was found to increase all variants by 5 fold, increase isoform 1 by 2.8 fold, increase isoform 2 by 1.7 fold, and increase isoform 3 by 3.7 fold in the first biological replicate (**Fig. 21B**), but did not change *mKCNN2* capturing all potential splicing variants and any specific splicing variants expression levels in three biological replicates (**Fig. 21C**).

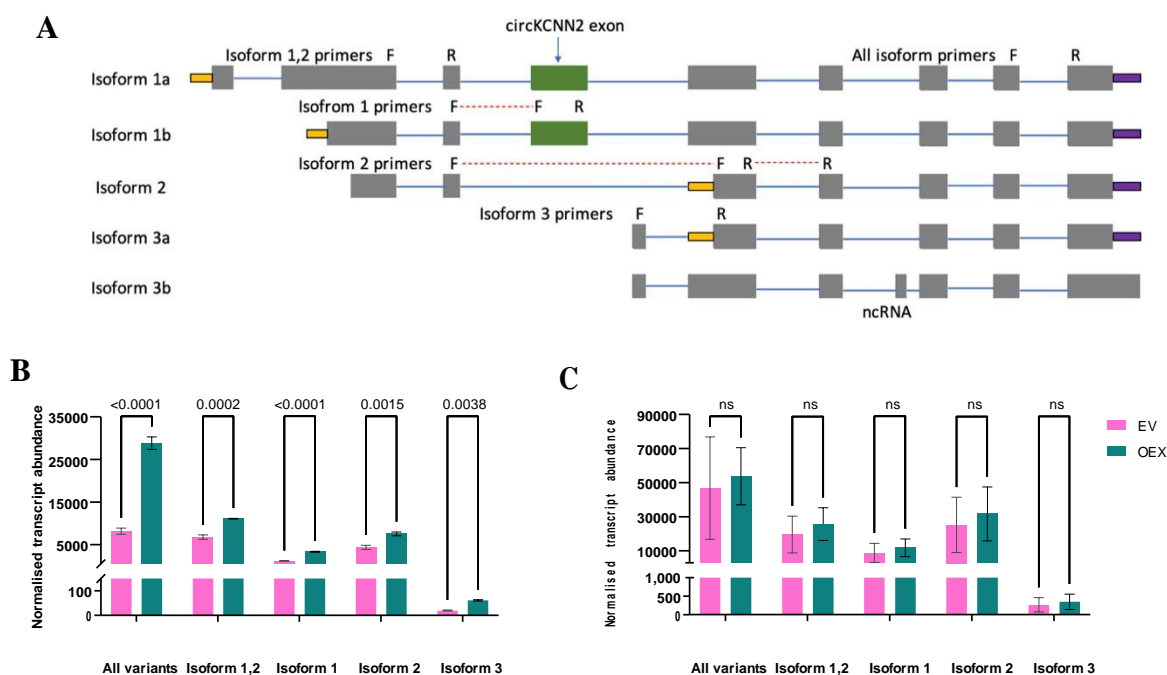


**Figure 21: Changing the level of *circKCNN2(8)* abundance increases the *mKCNN2* expression level in U87 cells in the first biological replicate.** (A) Representation of *KCNN2* mRNA isoforms. *CircKCNN2(8)* is generated from the backsplicing of exon 8 (green box), the same exon that is splicing out from *KCNN2* isoforms 2 and 3. All isoform primers were designed to detect all *KCNN2* splicing variants and isoform-specific primers were designed to detect the isoforms of interest. The grey boxes represent the coding exons, and the blue lines represent introns. The dotted red lines are the primers spanning from one exon to the next exon. The yellow boxes are protein start sites, and the purple boxes are protein stop sites. (B) qRT-PCR validation of all variants and specific isoform expression levels after the first overexpressing *circKCNN2(8)* in U87 cells. (C) qRT-PCR validation of all variants and specific isoform expression levels after overexpressing *circKCNN2(8)* in U87 cells within three biological replicates. Data has been normalised based on the ratio of TBP copies between EV and OEX, presented as mean  $\pm$  standard deviation. Statistical significance was determined by multiple t-tests. (N=3; 9) (P-value < 0.05, statistical significance; nc: no statistical significance; EV: empty vector; OEX: overexpressing).

### 3.4.7 Western blot to detect *KCNN2* protein

Given the change in mRNA abundance for *KCNN2*, including splice variants in the first biological replicate, it was decided to look at the levels of *KCNN2* proteins by Western blot.

Anti-KCNN2 antibody (Sigma-Aldrich) is able to detect two different protein variants, of ~30 kDa and ~60 kDa (full-length) respectively, representing two splice variants of KCNN2. For optimizing the anti-KCNN2 antibody concentration, proteins extracted from HL60 and HEK293 cells provided by Prof. Simon Conn were used for testing the different concentrations of anti-KCNN2 antibody (1:500; 1:1,000 and 1:2,000). Since there were no differences in the banding pattern, or intensities using different dilutions of the antibody (**Fig. 22**), I followed the manufacturer's recommendation of using 1:1000 for detecting the KCNN2 protein in transfected U87 cells.

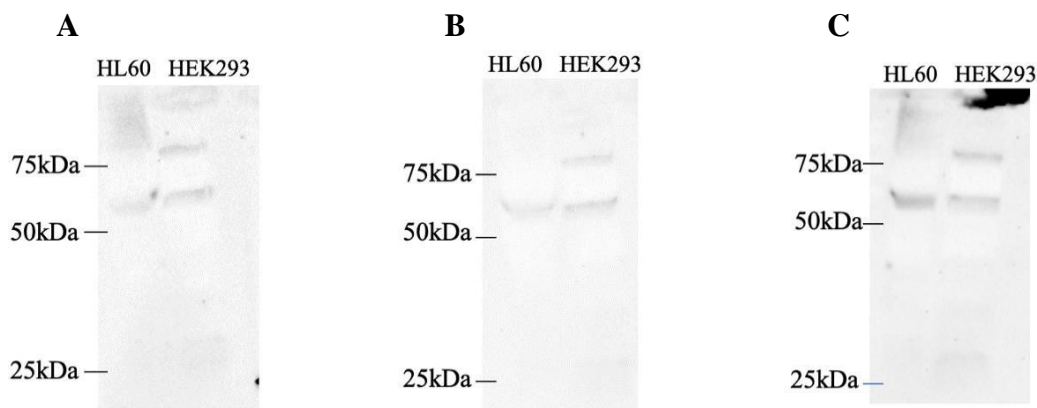


**Figure 22: Detecting KCNN2 protein with different concentrations of anti-KCNN2 antibody.** Antibody was diluted in (A) 1: 500; (B) 1:1,000; (C) 1:2,000.

As the *mKCNN2* (*exons 12-13*) expression level was increased after overexpressing *circKCNN2(8)* in U87 cells, two technical replicates from the first biological replicate were conducted to detect KCNN2 abundance (**Fig. 23A**). Another band strong band sitting at at ~35kDa was detected, but as these were absent in HL60 and HEK293 cells, it was deemed to be a non-specific band. Proteins with the correct size were analysed using total protein normalization to normalise between lanes (Appendix VI), there was no detectable change in either KCNN2 variant protein (**Fig. 23B**).

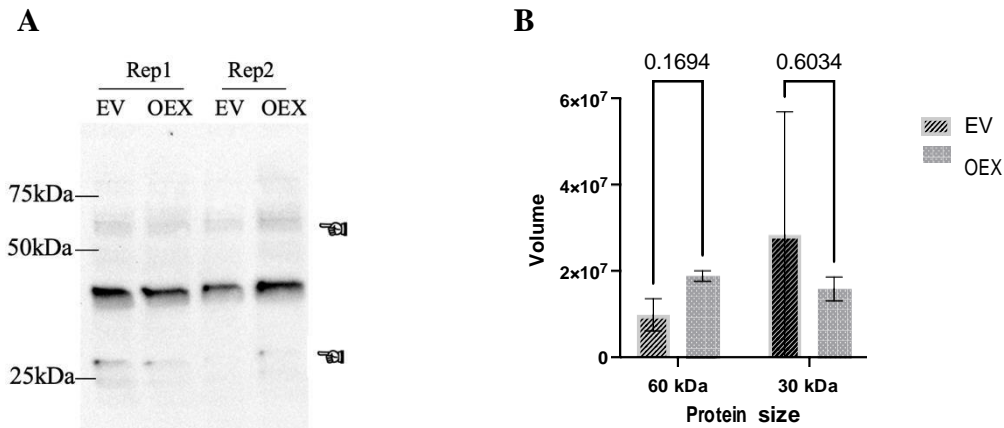


**Figure 23: Western blot of KCNN2 in U87 cells with overexpression of *circKCNN2(8)*.**

(A): Western blot image probed with anti-KCNN2 antisera at 1:1000 dilution. Molecular weights are shown using protein standards. (B): quantification of KCNN2 band intensity, normalised using total protein normalization (Appendix VI). Data presented as mean  $\pm$  standard deviation. Statistical significance was determined by multiple t-tests. (N=2, *P-value* < 0.05: statistical significance).

#### 3.4.8 qRT-PCR validation of nuclear/cytosolic fractionation

While circRNAs are largely found concentrated within the cytoplasm, it was important to determine the subcellular localization of each circRNA in this study. To validate the nuclear/cytosolic fractionation, the non-coding RNA, *MALAT1*, was used as a nuclear control, while *GAPDH* is an mRNA highly enriched in the cytoplasm, and was used as a cytosolic control. Performing nuclear: cytosolic fractionation of RNA in U87 with *circNFASC(26,27)* transfected line, followed by input of the same molar ratio of nuclear RNA: cytoplasmic RNA into the reverse transcription reactions, qRT-PCR demonstrated that both controls are enriched in the correct fraction. Secondly, all three circRNAs were found to be more abundant in the cytoplasm compared to the nucleus, but *circKCNN2(8)* and *circNFASC(26,27)* are not as highly enriched in the cytoplasm, suggesting they may play a role in the nucleus (Fig. 24).

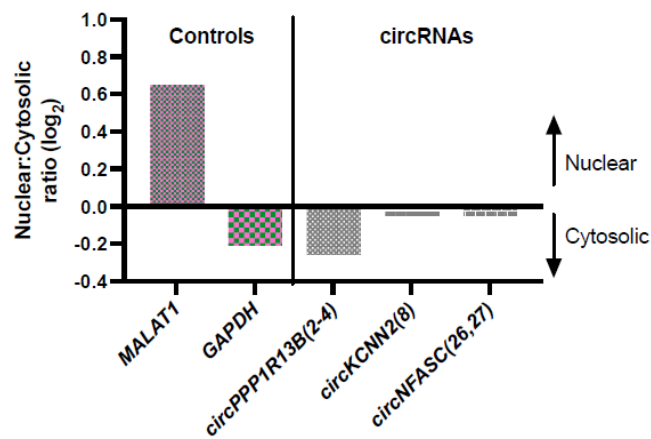


**Figure 24: qRT-PCR validation of nuclear/cytosolic fractionation of U87 cells.** All samples were expressed in both the nucleus and cytoplasm, *circPPP1R13B(2-4)* has higher expression in cytoplasm, while *circKCNN2(8)* and *circNFASC(26,27)* have nearly equal expression nucleus and cytoplasm. The results were presented as the ratio of average Ct value (N=3) between nucleus and cytoplasm.

### 3.5 cell assays

#### 3.5.1 Cell proliferation

A commonly measured parameter following transgenic manipulation of cells by circRNAs is cell proliferation or cell growth rate. For adherent cells, like U87 and U251, cell growth can be quantified by either cell confluence or nuclei counts. However, the GBM cells used herein have very faint edges that the software poorly recognise (Appendix VII, A), so nuclei counts were used to analyse the cell growth rate based on cell numbers, not cell size.

U251 cells overexpressing *circPPP1R13B(2-4)* showed a statistically significant increase with  $P$ -value = 0.0012 in cell proliferation of 13% compared to EV control cells in the first biological replicate (**Fig. 25A, G**). However, no difference in growth rate was seen for the *circNFASC(26,27)* or *circKCNN2(8)*. As a result, two additional biological replicates of *circPPP1R13B(2-4)* in U251 cells were generated and the growth assay was repeated. The initial increase seen for the first biological replicate was not found across all three biological replicates (**Fig. 25B, C**).

Cell proliferation in U87 cells overexpressing *circNFASC(26,27)* lines was 23% slower than EV control cells in the first biological replicate (**Fig. 25D**). However, overexpressing *circPPP1R13B(2-4)* and *circKCNN2(8)* respectively in U87 cells had no impact on cell proliferation. Performing two additional biological replicates of *circNFASC(26,27)* in U87 cells, the change in proliferation for the first replicate was not recapitulated in the second and third biological replicates (**Fig. 25E, F**), indicating *circNFASC(26-27)* overexpression in U87 cells is not significantly affecting cell growth rate.

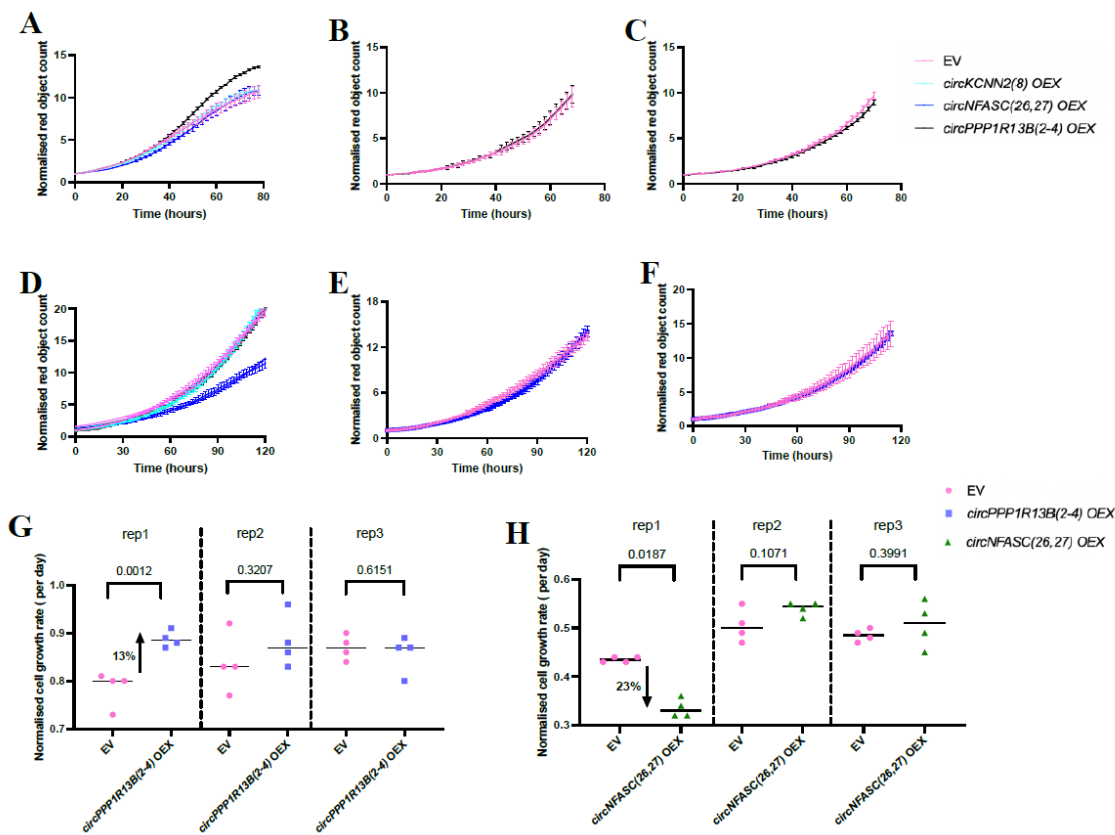


**Figure 25: Cell growth rate analysis based on nuclei counts.** (A-C) U251 transfected cells with biological replicate 1-3. (D-F) U87 transfected cells with biological replicate 1-3. The pink lines are EV control cells; the light blue lines are *circKCNN2(8)* overexpressing cells; the blue lines are *circNFASC(26,27)* overexpressing cells; and the black lines are *circPPP1R13B(2-4)* overexpressing cells. The data have been normalised based on the seeding numbers in each well (~ 2000 cells/well). (G) growth rate comparison between EV and *circPPP1R13B(2-4)* transfected U251 cells with three biological replicates. (H) growth rate comparison between EV and *circNFASC(26,27)* transfected U87 cells. Cell growth rates were calculated by normalised nuclei counts at exponential growth phase 20-hour window of

linear growth. The pink circles are EV control cells; the purple squares are *circPPP1R13B(2-4)* transfected U251 cells; and the green triangles are *circNFASC(26,27)* transfected U87 cells. Statistical significance was determined by two-way ANOVA (n=4 technical replicates per line; Mean  $\pm$  SD per well).

To understand the source of the differences between the first biological replicate and the second and third replicates for the two cell lines - *circPPP1R13B(2-4)* in U251 cells and *circNFASC(26,27)* in U87 cells – the maximum growth rate calculated from a 20hr window of exponential growth phase for each of the growth curves (**Figs 25A-F**) was plotted. It clearly demonstrated differences between the three replicates of empty vector lines in the U251 model and differences between the three overexpression lines in the U87 model that contributed to the growth curve differences (**Figs 25G,H**).

### 3.5.2 Colony formation assay

Soft agar colony formation assay is used to measure the ability of a single cell to form a colony without a solid anchoring matrix and is considered a reliable *in vitro* approach for assessing the oncogenicity of a cancer cell (Du et al., 2017). Given the impact on cell proliferation in the first biological replicate of *circPPP1R13B(2-4)* in U251 cells and *circNFASC(26,27)* in U87 cells, this assay was conducted on these cell lines with EV control (n=6 technical replicates). In U251 cells (**Fig. 26A, B**), overexpressing *circPPP1R13B(2-4)* lines had a statistically significant reduction of colony numbers by 36% after 14 days. Once colonies were formed, the cells grew faster by 4%, as indicated by the average volume of each colony, in *circPPP1R13B(2-4)* overexpressing lines compared to EV lines, which is consistent with cell growth rate (**Fig. 25A**). In U87 cells, overexpressing *circNFASC(26-27)* can largely reduce the cell's ability to form colonies by 29%, but cells grew faster by 13% compare to EV control cells once cell colonies formed (**Fig. 26C, D**).

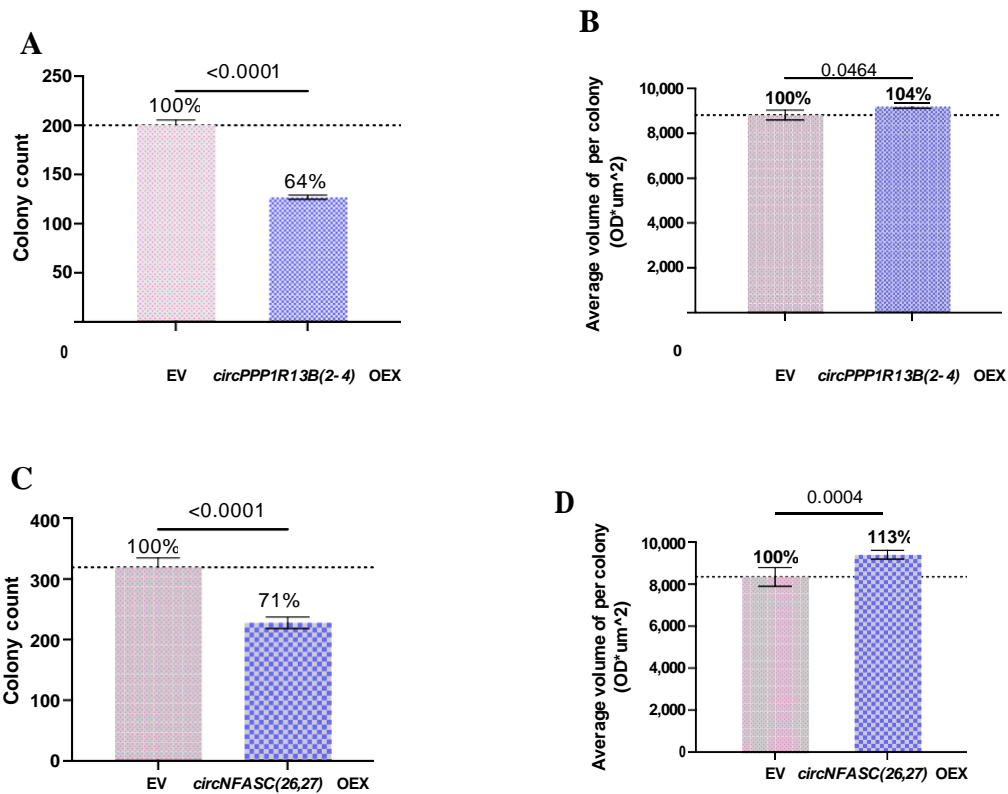


**Figure 26: Soft agar colony formation assay measuring colony counts and average colony volume in U251 cells (A, B) and U87 cells (C, D).** Data were shown as mean ± standard deviation and statistical significance was determined by unpaired t-tests (N= 6).

### 3.5.3 Cell morphology

Cell morphology is an important phenotypic measure of cancer cell lines and was assessed by utilising cellular marker stains in combination with a high-content imaging system, the Operetta CLS (Perkin Elmer). The stains used were DAPI which labels DNA to identify nuclei; Phalloidin: staining F-actin filaments which is used to identify the cytoskeleton (to measure cell length and width); CellTracker Deep Red: staining the cytoplasm to image cytoplasm and cellular area (Appendix VII, B).

Because of our limited access to the Operetta CLS imager, the assay was conducted with a single biological replicate of a limited number of cell lines which included *circPPP1R13B(2-4)* in U87 cells and *circNFASC(26,27)* and *circKCNN2(8)* in U251 cells (n=6 technical replicates, comprising approximately 6,000 cells). The image analysis was performed by Dr

Brett Stringer at SAHMRI. In U251 cells (**Fig. 27A-B**), transfection with *circPPP1R13B(2-4)* did not affect the nucleus or cell area compared with EV control cells. Meanwhile, the other parameters of cells, nucleus length and width, cell length and width, also did not change after *circPPP1R13B(2-4)* transfection (Appendix VIII).

In U87 cells (**Fig. 27C-F**), *circNFASC(26-27)* overexpression increased nucleus area by 27% ( $P$ -value = 0.0195) (**Fig. 27C**) and cell area by 64% ( $P$ -value = 0.0224) (**Fig. 27E**). Both of these increases were due to greater length of nuclei (20%, **Fig. 27D**) and cells (30%, **Fig. 27F**). Similarly *circKCNN2(8)* in U87 cells demonstrated a significant increase of 37% compared with EV control cells in the cell area (**Fig. 27E**), and the larger cell size is because of the longer cell length, which has been increased by 20% ( $P$ -value = 0.0003) (**Fig. 27F**).

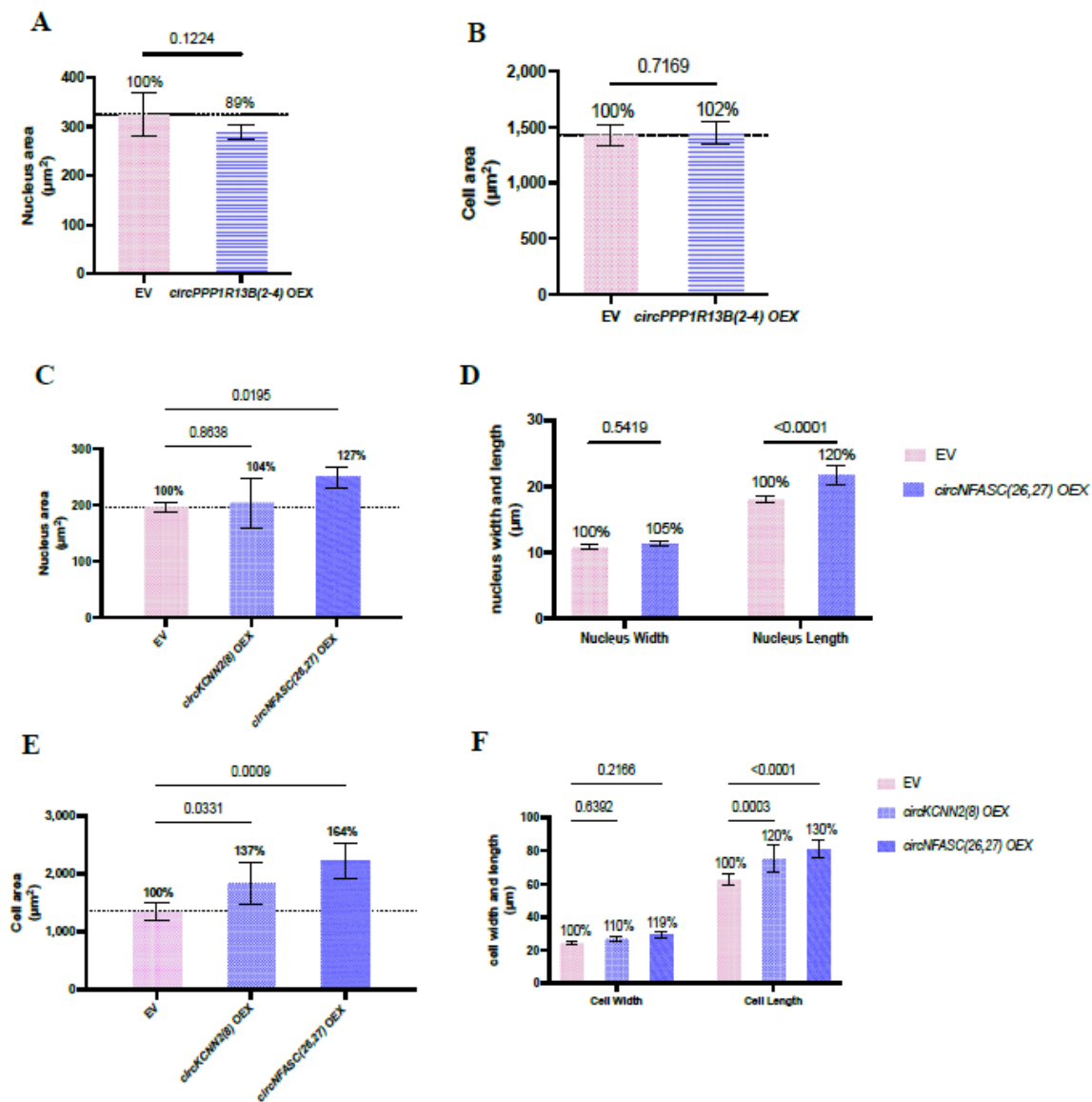


**Figure 27: Cell morphology observation after transfecting cells. (A, B)** nuclear area and cell area comparison in U251 transfected cells. **(C-F)** nucleus area, nucleus width and length, cell area, and cell length and width observation in U87 transfected cells. Data were displayed as Mean with standard deviation (N=6). Statistical significance was determined by one-way ANOVA. ( $P$ -value < 0.05, statistical significance).

### 3.5.4 miRNA prediction

A number of circRNAs have been demonstrated to be able to sponge miRNAs to regulate gene expression (Zhang et al., 2013). To illuminate if the three circRNA candidates studied

herein can bind to any miRNAs, and then impact their network of target transcripts, the Micro Target Prediction Database (MiRDB) was used for the downstream analysis (**Table 6**).

The predictions of miRNA targets are based on the entire circRNA sequence, with no specific miRNAs being predicted to bind to splice junctions of circRNA candidates. For each circRNA candidate investigated, a single miRNA is predicted to bind to the exon portion of the circRNA, therefore both mRNAs and circRNAs are potential targets of these miRNAs. Of these miRNAs, no perfect homology is predicted, with only 8 base pairs of the miRNAs in each case to potentially bind to the circRNA candidates. Although the number of homology sites among these three circRNA candidates (*circNFASC(26,27)*, *circPPP1R13B(2-4)* and *circKCNN2(8)*) is the same, the target score is different (the higher target score means the higher possible miRNAs target circRNAs), which is due to the different lengths of miRNAs, the stability of individual base pairs between miRNAs and target RNAs and also secondary structure of miRNAs. G-C base pairs have three hydrogen bonds, while A-T base pairs have two, so more G-C connections, a higher target score. Investigation of the other miRNA target genes was undertaken, with no related functions in GBM progression, however, these genes are enriched in brain tissues.

**Table 6: Predicted targets miRNA for circRNA candidates and possible functions of circRNAs.**

circRNA candidates	target miRNA name	target score	Numbers of potential base pair interactions	predicted targets for miRNA	gene function
<i>circNFASC (26-27)</i>	hsa-miR-1247-3p	94	8/24	LRFN1	Predicted to be involved in the regulation of the postsynaptic density assembly (Medicine, 2023).

<i>circPPP1R13B(2-4)</i>	hsa-miR-6841-3p	83	8/21	CCSAP	Regulate the formation of bipolar spindles during mitosis (Ohta et al., 2015).
<i>circKCNN2(8)</i>	hsa-miR-939-3p	93	8/21	BTRC	Mediate the ubiquitination (Westbrook et al., 2008).

Note: The higher target score, the higher possible miRNAs target circRNAs.

### 3.5.5 CircRNA database analysis

During this research project, I developed skills in bioinformatic and statistical analyses. As a result, I was able to reanalyse the circRNA dataset available at the outset of my project. I generated a volcano plot (**Fig. 28**), which is a common way to visualize differently expressed genes with fold change and *P*-value (McDermaid et al., 2019). There are 82,050 circular RNAs in this dataset including 76,683 non-statistically significant circular RNAs with fold change  $\leq 2$ . 3,647 circular RNAs are downregulated in GBM, and 1,719 circular RNAs are upregulated in GBM. Meanwhile, 113 circRNAs with *P*-value  $< 0.01$  ( $-\log_{10}p > 2$ ) are statistically significant with 65 circRNAs that are downregulated in GBM and 48 upregulated circRNAs in GBM.

If I had performed this analysis at the beginning of my research project, I may have selected different circRNAs, such as *circNELLI(9-11)*, *circAKT2(4,5)* and *circCNTNAP5(2,3)*, as there are clear standouts. However, circNFASC (exons 26-27) remained a good candidate since its expression level was 67.5-fold higher in healthy brain tissue than in GBM tumour with a *P*-value = 0.008. For the three potential selections: *circNELLI(9-11)* expressed a 52-fold higher with a *P*-value = 0.009, *circAKT2(4,5)* expressed a 44-fold higher with a *P*-value = 0.002, and *circCNTNAP5(2,3)* expressed a 32-fold higher with a *P*-value = 0.008 in healthy brain tissue than in GBM tumour.



4) in U251 cells and *circNFASC(26,27)* in U87 cells reduced the *in vitro* GBM cell line oncogenic potential and influenced cellular morphology, thus proving the project hypothesis.

Overexpressing circRNAs in cells is associated with a number of challenges, including the production of incorrectly spliced products, including *trans*-splicing products comprising concatemeric, head-to-tail linear RNAs. Digestion of RNA from cells with overexpression of the transgenic circRNAs with RNase R coupled with non-saturating RT-PCR is considered best practice for evaluating circRNA fidelity (Nielsen et al., 2022). In this project, it was demonstrated that the majority of circRNA product was circular, not *trans*-spliced linear RNAs as the RT-PCR bands were not significantly altered between digested and undigested samples. However, it was apparent that the linear *PPP1R13B* mRNA was not fully digested following RNase R treatment. This is unlikely to be a result of technical error as both other mRNAs were almost entirely degraded under the same conditions. It is more likely that the *PPP1R13B* mRNA possesses sufficient RNA base pairing or secondary structure in the region which was amplified by RT-PCR which reduces and, in some cases, completely resists RNase R digestion (Xiao and Wilusz, 2019).

For completing the phenotypic and transcriptional analyses, the three chosen circRNAs were stably overexpressed in commonly used GBM cell lines, U251 and U87. All circRNAs were successfully overexpressed in both cell lines at very high levels, which may have caused some non-specific effects as opposed to lower expression levels. While cell proliferation can be calculated by either phase confluence (cell area) or nucleus counts (cell numbers), due to cell size difference seen for some of the cell lines, combined with the inability of InCucyte software to recognize cell edges properly, nucleus counts were used for cell proliferation analysis. Different growth effects, or lack thereof, were observed by overexpressing the same circRNAs in different cell lines (U251 and U87) in the first biological replicate. For example, *CircPPP1R13B(2-4)* increased cell growth rate by 13% in U251 cells, while no detectable changes were observed in U87 cells. Although both cell lines are glioma cell lines, U251 is a p53 mutant cell line, while U87 is a p53 wild-type cell line (Lee et al., 2020). P53 is a major tumour suppressor gene that selectively eliminates mutated or damaged cells, and it regulates transcriptional target genes involved in many cellular responses including cell cycle, DNA repair, cell proliferation, and apoptosis, among others (Lee et al., 2020). The GBM patients

with P53 mutations have a worse prognosis and response to the standard treatment, the Stupp protocol (Wang et al., 2014). Therefore, the p53 mutational status, among other genetic and metabolic differences (Arthurs et al., 2020), could have contributed to the difference seen between cell lines, especially for *circNFASC(26,27)* which is not present in either cell line, but whose overexpression reduced cell proliferation in U251 but not U87 cells.

Given the short amount of time for this research project, it was decided to perform a single biological replicate for each three circRNA (and empty vector control) in both U251 and U87 GBM cell lines and then follow up on the most interesting results with three biological replicates. The additional biological replicates did not identify a consistent trend as with the first replicate and overall showed no alteration in cell proliferation. It is possible that this results from the first biological replicate being cultivated for more than 1.5 months before undertaking the cell proliferation assay, as higher passage numbers of cells are known to affect the growth rate (Cao et al., 2021). By comparing the three biological replicates, we found that long-term cultivation has the potential to alter cell proliferation. The growth rate of U87 transfected *circNFASC(26,27)* cells in the first biological replicate was 680 cells/day, while in the biological replicate 2 and 3 were 1,080 cells/day and 1,020 cells/day respectively. In both EV control cells, the biological replicate 1 (U251, EV: 1,580 cells/day; U87, EV: 880 cells/day) also grew slower than biological replicate 2 (U251, EV: 1,680 cells/day; U87, EV: 1,000 cells/day) and 3 (U251, EV: 1,740 cells/day; U87, EV: 980 cells/day).

Another surprising result was seen for the overexpression of *circKCNN2(8)* in U87 cells which showed an increase in *mKCNN2* expression level. Despite this, the increase was not seen in biological replicates 2 and 3. By probing the qRT-PCR results of three biological replicates, we observed the issue was more likely with replicate 1 of the EV line as there were fewer *mKCNN2* copies (8,192 copies) in the first biological replicate than in replicates 2 and 3 (50,502 and 81,515 copies respectively). It is possible that this results from the removal of G418 selection pressure (for the minicirc2 plasmid) after three weeks of culture. G418 is an aminoglycoside related to gentamicin, which is a potent stop codon suppressor (Stepanenko and Heng, 2017). It has been found endogenous heme oxygenase 1 (HO1) expression was significantly increased in human renal proximal tubule cells transfected with pcDNA3 vector

and treated with G418 (250 µg/ml) or treated with G418 alone (50-500 µg/ml) without plasmid transfection (Shiraishi et al., 2001). This finding might also explain why the mKCNN2 expression level in EV lines was different in the first biological replicate. It was seen by Western blot using KCNN2 antisera that the KCNN2 protein was not consistently altered, using total protein normalisation.

The cell lines showing proliferation changes in the first biological replicate triggered further phenotypic investigation, so colony formation assay and cell morphology assay were conducted but with a single biological replicate due to research time restriction. There seems no correlation between cell proliferation and colony formation assay since the changes in cell growth rate have not been found to have consistent changes in either colony numbers or average volume per colony. In U251, *circPPP1R13B(2-4)* transfected lines, cells grow faster, and bigger but fewer colonies were formed, while, in U87, *circNFASC(26,27)* transfected lines, cells grow slower, and bigger but fewer colonies were formed. However, there are some correlations between cell morphology changes and colony formation. The bigger size cells with a bigger nucleus can reduce the number of colonies, which means the bigger cells can reduce tumorigenicity, but this correlation was only found in U87 with *circNFASC(26,27)* overexpressing lines, so this correlation needs to be further confirmed. There is no literature that has found how the sizes of cells or nuclei affect tumorigenicity.

Recent work in our laboratory produced mRNA-seq libraries on the same samples for which we had the published circRNAseq dataset. If this data was available earlier, it would have been possible to look at changes in the abundance of circRNA relative to the parental mRNA. By combining this with knowledge on the nuclear: cytoplasmic distribution and improved bioinformatic analyses on expression difference may have created an even higher confidence list of circRNAs to analyse. In general, the expression level of circRNAs is proportional to that of their cognate mRNA expression level and most circRNAs are enriched in the cytoplasm (Yang et al., 2021), therefore, the circRNAs with an inverse relationship with their cognate mRNA may be more likely to play a functional role in GBM.

## **5. Limitations of this study**

The first limitation of this study was the database used for the selection of circRNA candidates. Although the database established in our laboratory analysed five healthy brain tissues and five GBM tumours, only two samples are matched (from the same patient). The ideal method of distinguishing differently expressed circRNAs would be to use all matched samples and a much larger cohort size would improve the confidence in circRNA candidates for investigation.

The second limitation of this project was the cell lines used. Whilst the U251 cell line and U87 cell line provide an excellent model to validate all experiments performed, and both cell lines are commonly used for GBM study, the ideal cell model would be using patient-derived cell lines from GBM patients. While these cell lines are available in our laboratory the cost and difficulty in handling and obtaining transgenic lines were considered too high and so U251 and U87 lines were utilised for this short-term project and basic circRNA functional investigation. Additional models that could be employed in future would include organoids, or *in vivo* models where human cell lines are xenografted into immunocompromised mice. As mice do not normally present with GBM, there is a possibility of using immunocompetent mice, but this would require using mouse brain cells which are modified to include mutations in the orthologues of genes commonly mutated in human GBM.

The last major limitation is the time limitation of this research project. It was a 10-month period, so there was not enough time to examine the higher confidence circRNAs from the volcano plot I generated at the end of my research project. Also, I was unable to complete three biological replicates of all lines and also the colony formation and cell morphology assays, however, it is worth repeating these two experiments for verifying the phenotypic changes that have been observed in a single biological replicate.

## **6. Future directions**

Although the criteria for selecting candidate circRNAs in this project was not perfect, only based on fold change of five healthy brain tissue and five GBM tumours, there were still

phenotypic changes which arose following overexpression, indicating circRNAs play a functional role in GBM. In the established volcano plot, there are 113 differently expressed circRNAs with a  $P$ -value  $< 0.01$ , which gives us a valuable shortlist of circRNA candidates for future investigation. It may be possible to perform high-throughput knockdown of these circRNAs in a library format by either CRISPR-Cas13b/d-mediated circRNA knockdown, or shRNA-based screening to study cell proliferation.

Fewer colonies being formed in soft agar assays, an *in vitro* model of cellular tumorigenicity and anchorage-independent growth, in transfected cells also could justify further investigation in other models, including 3-dimensional organoids, or ideally animals for checking tumorigenicity *in vivo*. Meanwhile, cell morphology changes also guide us to explore more, such as cell migration assay for checking the effects of cell size and shape on cell mobility. More functional investigation of circRNAs will give us a better understanding of GBM, thus guiding us to potentially find a biomarker for early detection or a molecular therapeutic target to improve treatment.

## Appendix 0

The list of publications that I contributed during this research project (my name in bold).

1. Shiu, P.K.T.; Ilieva, M.; Holm, A.; Uchida, S.; DiStefano, J.K.; Bronisz, A.; Yang, L.; Asahi, Y.; Goel, A.; Yang, L.; Nuthanakanti, A.; Serganov, A.; Alahari, S.K.; Lin, C.; Pardini, B.; Naccarati, A.; Jin, J.; Armanios, B.; Zhong, X.-b.; Sideris, N.; Bayraktar, S.; Castellano, L.; Gerber, A.P.; **Lin, H.**; Conn, S.J.; Sleem, D.M.M.; Timmons, L. The *Non-Coding RNA* Journal Club: Highlights on Recent Papers—12. *Non-Coding RNA* **2023**, *9*, 28. <https://doi.org/10.3390/ncrna9020028>
2. Gantley, L.; Stringer, B.W.; Conn, V.M.; Ootsuka, Y.; Holds, D.; Slee, M.; Aliakbari, K.; Kirk, K.; Ormsby, R.J.; Webb, S.T.; Hanson, A.; **Lin, H.**; Selth, L.A.; Conn, S.J. Functional Characterisation of the Circular RNA, *circHTT(2-6)*, in Huntington’s Disease. *Cells* **2023**, *12*, 1337. <https://doi.org/10.3390/cells12091337>
3. Conn, V.M.; Gabryelska, M.; Toubia, J.; Kirk, K.; Gantley, L.; Powell, J.A.; Cildir, G.; Marri, S.; Liu, R.; Stringer, B.W.; Townley, S.; Webb, S.T.; **Lin, H.**; Samaraweera, S.E.; Bailey, S.; Moore, A.S.; Maybury, M.; Liu, D.; Colella, A.D.; Chataway, T.; Wallington-Gates, C.T.; Walters, L.; Sibbons, J.; Selth, L.A.; Tergaonkar, V.; D’Andrea, R.J.; Pitson, S.M.; Goodall, G.J.; Conn, S.J. Circular RNAs drive oncogenic chromosomal translocations within the MLL recombinome in leukemia. *Cancer Cell* **2023** <https://doi.org/10.1016/j.ccell.2023.05.002>

## Appendix I

Gblock assembly sequence for overexpressing circRNA candidates.

Gene		<i>circNFASC(26-27)</i>	<i>circKCNN2(8)</i>	<i>circPPP1R13B(2-4)</i>
5' primer	M13F	GTAAAACGACGGCCAG	GTAAAACGACGGCCAG	GTAAAACGACGGCCAG
5' RE	BsmB I	tcagGgagacg	tcagGgagacg	tcagGgagacg
Sequence		CCCCTGATGAGCAGTCCATATGGA ACGTCACGGTGCTCCCCAACAGTA AATGGGCCAACATCACCTGGAAG CACAATTTCCGGGCCCGAACTGAC TTTGTGGTTGAGTACATCGACAGC AACCATACGAAAAAACTGTCCC AGTTAAGGCCCAGGCTCAGCCTAT ACAGCTGACAGACCTCTATCCCGG GATGACATACACGTTGCGGGTTTA TTCCCGGGACAACGAGGGCATCA GCAGTACCGTCATCACCTTTATGA CCAGTACAG	TTGTTTCATGGTGGACAATGGAGCAGATGAC TGGAGAATAGCCATGACTTATGAGCGTATT TTCTTCATCTGCTTGAAATACTGGTGTGTG CTATTCATCCCATACCTGGGAATTATACATT CACATGGACGGCCCGGCTTGCCTTCTCTAT GCCCCATCCACAACCACCGCTGATGTGGAT ATTATTTTATCTATAACCAATGTTCCTTAAGAC TCTATCTGATTGCCAGAGTCATGCTTTTACA TAGCAAACCTTTTACTGATGCCTCCTCTAGA AGCATTGGAGCACTTAATAAGATAAACTTC AATACACGTTTTGTTATGAAGACTTTAATGA CTATATGCCCAGGAACTGTACTCTTGGTTTT TAGTATCTCATTATGGATAATTGCCGCATGG ACTGTCCGAGCTTGTGAAAAG	ATGATATTAAGTGTTCCTTGAG CAACAATGAACAGATTTTAACA GAAGTTCCTATAACACCGGAAA CAACCTGTCGAGATGTTGTAGA ATTTTGCAAGGAACCTGGAGAA GGCAGCTGCCATTTAGCTGAAG TGTGGAGGGGAAATGAACGTCC CATAACCTTTGATCATATGATGT ACGAACATCTTCAGAAATGGGG TCCACGGAGGGGAAGAAGTGAAA TTTTTCCTTCGACACGAGGACTC CCCAACTGAGAACAGTGAACAA GGTGGCCGTCAGACCCAAGAGC AACGAACTCAGAGAAAATGTAAT
3' RE	BsmB I	cgtctcGgtaa	cgtctcGgtaa	cgtctcGgtaa
3' primer	M13R	GTCATAGCTGTTTCCTG	GTCATAGCTGTTTCCTG	GTCATAGCTGTTTCCTG

## Appendix II

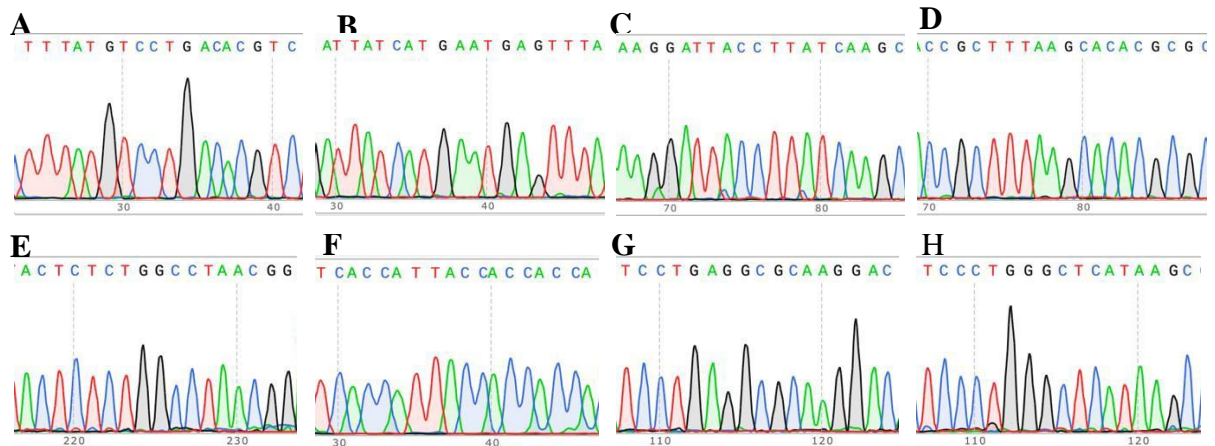
Function investigation of circRNA candidates and their parent gene.

ID in circBase	CircRNAs	Expression in Glioblastoma	Functions	Functions of parent gene
hsa_circ_0000940	<i>circMARK4(3-4)</i>	Overexpressed		Serine/threonine-protein kinase (Trinczek et al., 2004)
hsa_circ_0007948	<i>circGLIS3(2)</i>	Overexpressed	Significantly upregulated in TMZ-resistant glioma cells (Chi et al., 2022)	Could as an activator and repressor of transcription (Kim et al., 2003)
hsa_circ_0007948	<i>circPTPN13(22-25)</i>	Overexpressed		Tyrosine phosphatase which regulates negatively FAS-induced apoptosis and NGFR-mediated pro-apoptotic signalling (Villa et al., 2005)
hsa_circ_0001178	<i>circUSP25(2-3)</i>	Overexpressed		Deubiquitinating enzyme that hydrolyzes ubiquitin moieties conjugated to substrates (Valero et al., 1999)
hsa_circ_0005332	<i>circZBTB20(4)</i>	Overexpressed	Regulate homeostasis of innate lymphoid cells (ILCs) (Liu et al., 2021)	May be a transcription factor that may be involved in hematopoiesis, oncogenesis, and immune responses (Zhang et al., 2001)
hsa_circ_0005692	<i>circGLIS2(3,4)</i>	Overexpressed	Higher expression in colorectal cancer (CRC) tissue and cell line, and it can regulate cell migration (Chen et al., 2020)	Glis2 behaves as a bifunctional transcriptional regulator (Zhang et al., 2002)
hsa_circ_0001730	<i>circEPHB4(11-12)</i>	Overexpressed	Upregulated in gliomas tissues and cell lines (Jin et al., 2021)	Activation of EPHB4 results in forward signaling in the receptor-expressing cell (Erber et al., 2006)
hsa_circ_0073237	<i>circVCAN(3)</i>	Overexpressed		A negative regulator of chemokine function (Hirose et al., 2001)

hsa_circ_0073237	<i>circNFASC(26-27)</i>	Lower expressed		Playing a pivotal role in the development and function of the axon initial segment (AIS) (Smigiel et al., 2018)
hsa_circ_0111758	<i>circERC2(13-14)</i>	Lower expressed		In brain, <i>ERC2</i> is a subunit of the cytomatrix at the active zone (CAZ) protein complex, which is involved in neurotransmitter release (Takao-Rikitsu et al., 2004)
hsa_circ_0131933	<i>circMLIP(8-11)</i>	Lower expressed		
hsa_circ_0005791	<i>circPPP1R13B(2-4)</i>	Lower expressed	Promoting chicken skeletal muscle satellite cells (SMSCs) proliferation and differentiation (Shen et al., 2021)	May regulate the tumor suppression function of p53 in vivo (Samuels-Lev et al., 2001)
hsa_circ_0024997	<i>circERC1(14,15)</i>	Lower expressed		
hsa_circ_0127664	<i>circKCNN2(8)</i>	Lower expressed	The expression of <i>circKCNN2</i> (exon 8) was downregulated in hepatocellular carcinoma HCC tissues (Liu et al., 2022)	<i>KCNN2</i> expresses a potassium current that is sensitive to apamin, scyllatoxin, and tubocurarine and is insensitive to charybdotoxin (Desai et al., 2000)

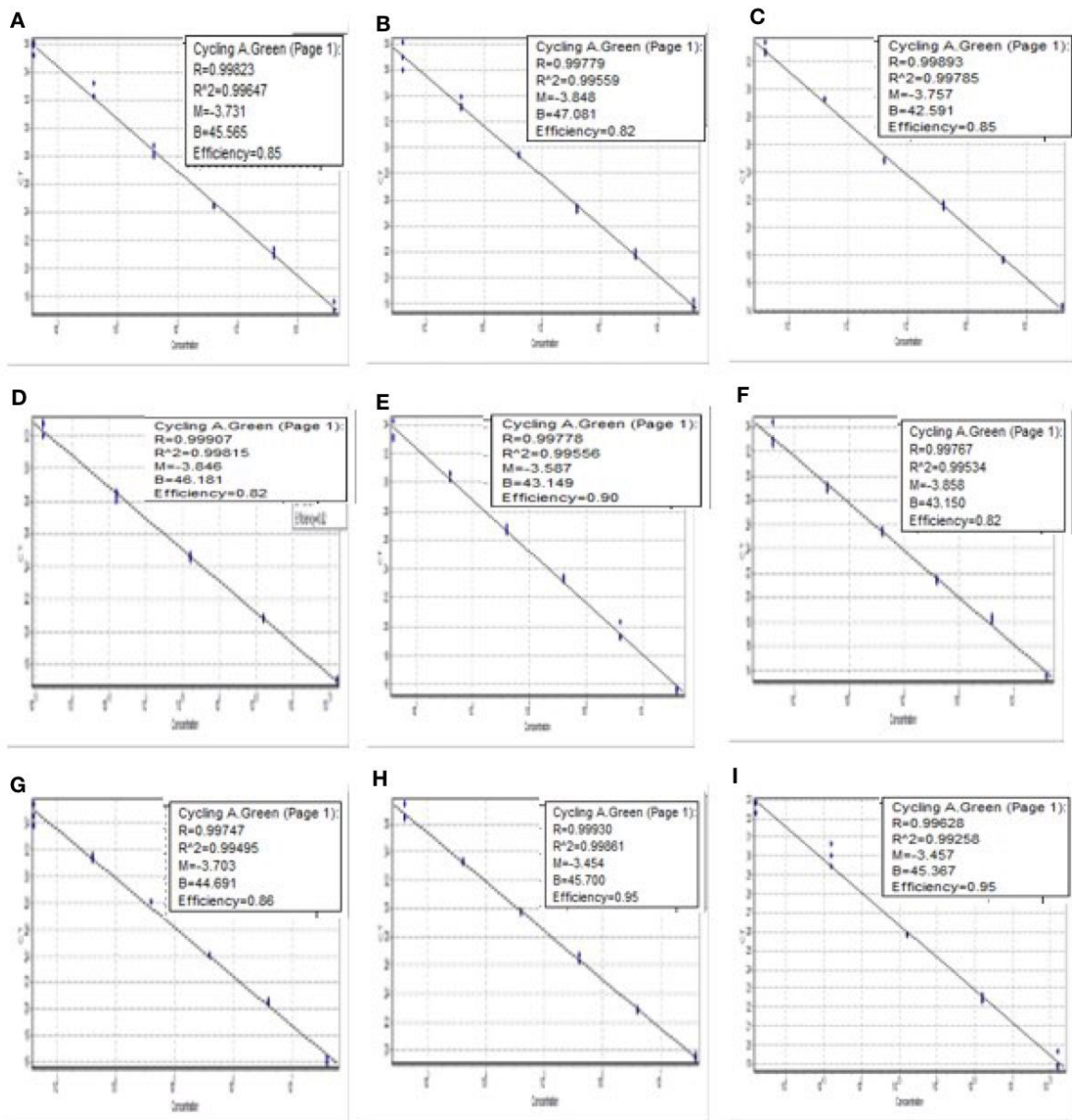
## Appendix III

Sanger sequencing results of circRNA candidates related to parental gene mRNA. A): *mPTPN13*(exon 45); B): *mUSP25* (exon 23); C): *mZBTB20* (exon12); D): *mGLIS 2* (exon8); E): *mNFASC* (exon 30); F): *mERC2* (exon16); G): *mPPP1R13B* (exon16); H): *mKCNN2* (exon13).



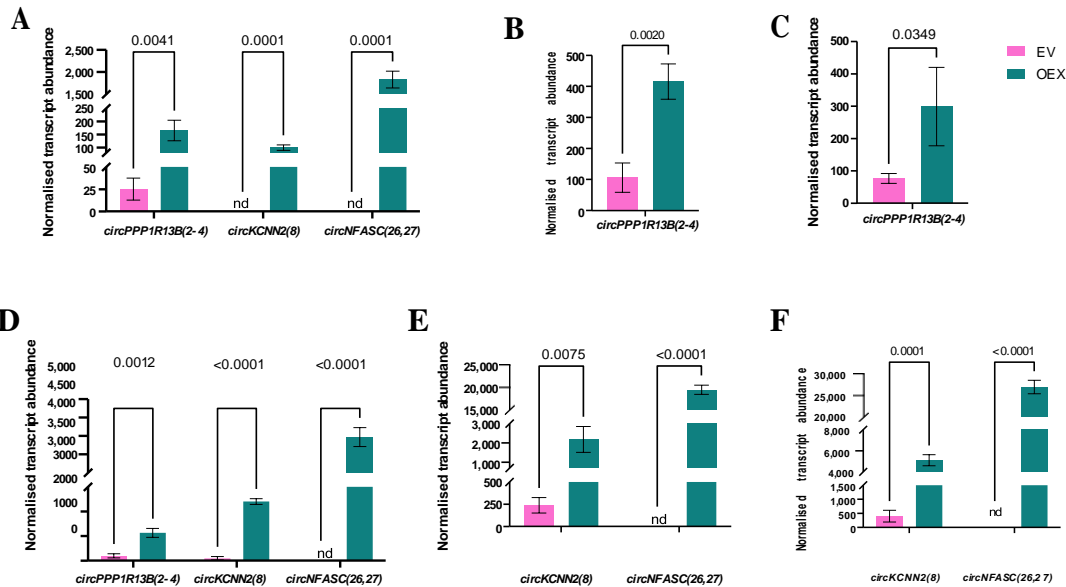
## Appendix IV

Standard curves were determined by qRT-PCR for each primer pair. Serial six ten-fold dilutions were performed, and the initial samples contained 40,000,000 copies. A): *circPPP1R13B(2-4)*; B): *circKCNN2(8)*; C): *circNFASC (26-27)*; D): *mKCNN2* (all isoforms; exons 12-13); E): *mKCNN2* (isoform 1,2; exons 6-7); F): *mKCNN2* (isoform 1; exons 7-8); G): *mKCNN2* (isoform 2; exons 7-10); H): *mKCNN2* (isoform 3; exons 1-2); I): *TBP* (exon 2).



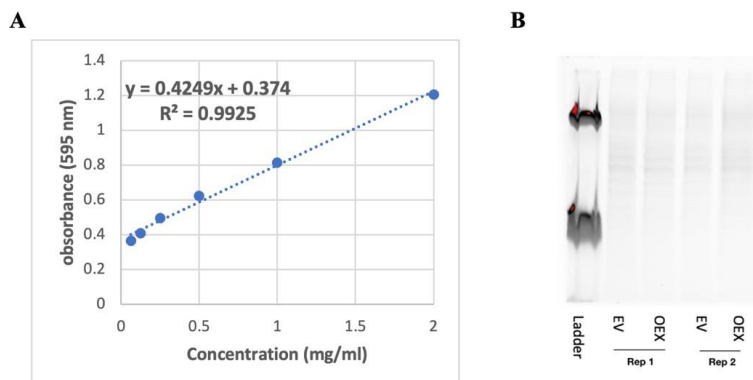
## Appendix V

QRT-PCR results after transfecting U251 cells (A-C: biological replicate 1-3) and U87 cells (D-F: biological replicate 1-3) with three biological replicates. Data has been normalised based on the ratio of TBP copies between EV and OEX. Statistical significance was determined by multiple *t*-tests. ( $P$ -value < 0.05: statistically significant; nd: non-detected).



## Appendix VI

Standard curve for determining protein concentration (A), and the image of total protein used for normalisation (B).

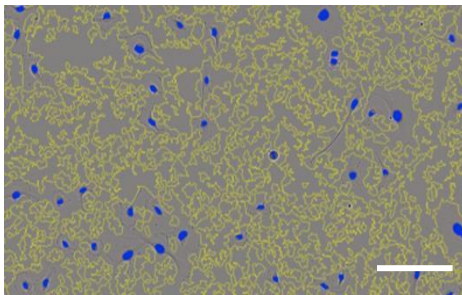


## Appendix VII

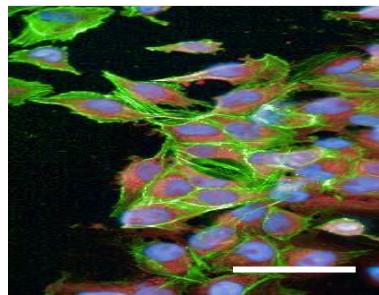
(A) Image was obtained from U251, EV cells at the 20th hour through the InCucyte SX5 system with 10X magnification, and the scale bar was 400  $\mu\text{m}$ . Nuclei were stained in blue, and the yellow lines circled the edge of cells.

(B) Image was obtained from U251 cells transfected by *circKCNN2(8)* through Operatta CLS system with 10X magnification, and the scale bar was 100  $\mu\text{m}$ . Cell nuclei were stained in blue, cellular areas were in red, and cell skeletons were in fluorescent green.

**A**

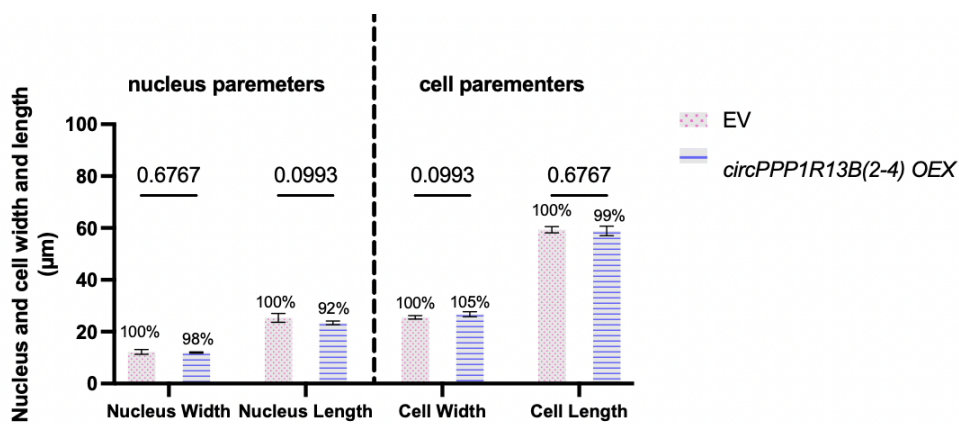


**B**



## Appendix VIII

Cell morphology analysis in transfected U251 lines (A) and U87 lines (B). Data were displayed as Mean with standard deviation (N=6). Statistical significance was determined by one-way ANOVA. ( $P$ -value < 0.05, statistical significance).



## 7. References

- ALPEN, K., VAJDIC, C. M., MACINNIS, R. J., MILNE, R. L., KOH, E. S., HOVEY, E., HARRUP, R., BRUINSMA, F., NGUYEN, T. L., LI, S., JOSEPH, D., BENKE, G., DUGUÉ, P. A., SOUTHEY, M. C., GILES, G. G., ROSENTHAL, M., DRUMMOND, K. J., NOWAK, A. K., HOPPER, J. L., KAPUSCINSKI, M. & MAKALIC, E. 2022. Australian genome-wide association study confirms higher female risk for adult glioma associated with variants in the region of CCDC26. *Neuro Oncol.*
- ANNOVAZZI, L., CALDERA, V., MELLAI, M., RIGANTI, C., BATTAGLIA, L., CHIRIO, D., MELCARNE, A. & SCHIFFER, D. 2015. The DNA damage/repair cascade in glioblastoma cell lines after chemotherapeutic agent treatment. *International journal of oncology*, 46, 2299-2308.
- ARTHURS, A. L., KEATING, D. J., STRINGER, B. W. & CONN, S. J. 2020. The suitability of glioblastoma cell lines as models for primary glioblastoma cell metabolism. *Cancers*, 12, 3722.
- BEGUM, S., YIU, A., STEBBING, J. & CASTELLANO, L. 2018. Novel tumour suppressive protein encoded by circular RNA, circ-SHPRH, in glioblastomas. *Oncogene*, 37, 4055-4057.
- BERNHARDI, R. V., BERNHARDI, L. E.-V. & EUGENÍN, J. 2017. What is neural plasticity? *The plastic brain*, 1-15.
- CAO, J., WU, X., QIN, X. & LI, Z. 2021. Uncovering the effect of passage number on HT29 cell line based on the cell metabolomic approach. *Journal of Proteome Research*, 20, 1582-1590.
- CHEN, B. J., HUANG, S. & JANITZ, M. 2019. Changes in circular RNA expression patterns during human foetal brain development. *Genomics*, 111, 753-758.
- CHEN, J., YANG, X., LIU, R., WEN, C., WANG, H., HUANG, L., LI, W., ZHU, Z., ZHU, Y. & LIU, H. 2020. Circular RNA GLIS2 promotes colorectal cancer cell motility via activation of the NF- $\kappa$ B pathway. *Cell death & disease*, 11, 1-13.

- CHEN, L. L., BINDEREIF, A., BOZZONI, I., CHANG, H. Y., MATERA, A. G., GOROSPE, M., HANSEN, T. B., KJEMS, J., MA, X. K., PEK, J. W., RAJEWSKY, N., SALZMAN, J., WILUSZ, J. E., YANG, L. & ZHAO, F. 2023. A guide to naming eukaryotic circular RNAs. *Nat Cell Biol*, 25, 1-5.
- CHI, G., XU, Y., CAO, X., LI, Z., CAO, M., CHISTI, Y. & HE, N. 2022. Production of polyunsaturated fatty acids by *Schizochytrium* (*Aurantiochytrium*) spp. *Biotechnology Advances*, 55, 107897.
- CLANCY, S. 2008. RNA splicing: introns, exons and spliceosome. *Nature Education*, 1, 31.
- CONN, S. J., PILLMAN, K. A., TOUBIA, J., CONN, V. M., SALMANIDIS, M., PHILLIPS, C. A., ROSLAN, S., SCHREIBER, A. W., GREGORY, P. A. & GOODALL, G. J. 2015. The RNA binding protein quaking regulates formation of circRNAs. *Cell*, 160, 1125-34.
- CONN, V. M., GABRYELSKA, M., MARRI, S., STRINGER, B. W., ORMSBY, R. J., PENN, T., POONNOOSE, S., KICHENADASSE, G. & CONN, S. J. 2020. SRRM4 Expands the Repertoire of Circular RNAs by Regulating Microexon Inclusion. *Cells*, 9, 2488.
- CONN, V. M., GABRYELSKA, M., TOUBIA, J., KIRK, K., GANTLEY, L., POWELL, J. A., CILDIR, G., MARRI, S., LIU, R., STRINGER, B. W., TOWNLEY, S., WEBB1, S. T., LIN, H., SAMARAWEERA, S. E., BAILEY, S., MOORE, A. S., MAYBURY, M., LIU, D., COLELLA, A. D., CHATAWAY, T., WALLINGTON-GATES, C. T., WALTERS, L., SIBBONS, J., SELTH, L. A., TERGAONKAR, V., D'ANDREA, R. J., PITSON, S. M., GOODALL, G. J. & CONN, S. J. in press. Circular RNAs drive oncogenic chromosomal translocations within the MLL recombinome in leukemia. *Cancer Cell*.
- CONN, V. M., HUGOUVIEUX, V., NAYAK, A., CONOS, S. A., CAPOVILLA, G., CILDIR, G., JOURDAIN, A., TERGAONKAR, V., SCHMID, M. & ZUBIETA, C. 2017. A circRNA from SEPALLATA3 regulates splicing of its cognate mRNA through R-loop formation. *Nature plants*, 3, 1-5.

- DA CRUZ, L. H., RODRIGUEZ, I., DOMINGUES, R., GASPARETTO, E. & SORENSEN, A. 2011. Pseudoprogression and pseudoresponse: imaging challenges in the assessment of posttreatment glioma. *American Journal of Neuroradiology*, 32, 1978-1985.
- DELGADO-LÓPEZ, P. & CORRALES-GARCÍA, E. 2016. Survival in glioblastoma: a review on the impact of treatment modalities. *Clinical and Translational Oncology*, 18, 1062-1071.
- DESAI, R., PERETZ, A., IDELSON, H., LAZAROVICI, P. & ATTALI, B. 2000. Ca<sup>2+</sup>-activated K<sup>+</sup> channels in human leukemic Jurkat T cells. Molecular cloning, biochemical and functional characterization. *J Biol Chem*, 275, 39954-63.
- DJEBALI, S., DAVIS, C. A., MERKEL, A., DOBIN, A., LASSMANN, T., MORTAZAVI, A., TANZER, A., LAGARDE, J., LIN, W. & SCHLESINGER, F. 2012. Landscape of transcription in human cells. *Nature*, 489, 101-108.
- DU, F., ZHAO, X. & FAN, D. 2017. Soft Agar Colony Formation Assay as a Hallmark of Carcinogenesis. *Bio Protoc*, 7, e2351.
- DU, W. W., YANG, W., LIU, E., YANG, Z., DHALIWAL, P. & YANG, B. B. 2016. Foxo3 circular RNA retards cell cycle progression via forming ternary complexes with p21 and CDK2. *Nucleic acids research*, 44, 2846-2858.
- ERBER, R., EICHELSBACHER, U., POWAJBO, V., KORN, T., DJONOV, V., LIN, J., HAMMES, H. P., GROBHOLZ, R., ULLRICH, A. & VAJKOCZY, P. 2006. EphB4 controls blood vascular morphogenesis during postnatal angiogenesis. *The EMBO journal*, 25, 628-641.
- FANG, L., DU, W. W., LYU, J., DONG, J., ZHANG, C., YANG, W., HE, A., KWOK, Y. S. S., MA, J. & WU, N. 2018. Enhanced breast cancer progression by mutant p53 is inhibited by the circular RNA circ-Ccnb1. *Cell Death & Differentiation*, 25, 2195-2208.
- FLORIS, G., ZHANG, L., FOLLESA, P. & SUN, T. 2017. Regulatory role of circular RNAs and neurological disorders. *Molecular neurobiology*, 54, 5156-5165.
- GABRIELA PICHARDO, M. 2020. *Brain Cancer and Gliomas* [Online]. [Accessed 29 September 2022].

- GAO, X., XIA, X., LI, F., ZHANG, M., ZHOU, H., WU, X., ZHONG, J., ZHAO, Z., ZHAO, K. & LIU, D. 2021. Circular RNA-encoded oncogenic E-cadherin variant promotes glioblastoma tumorigenicity through activation of EGFR–STAT3 signalling. *Nature Cell Biology*, 23, 278-291.
- GOODALL, G. J. & WICKRAMASINGHE, V. O. 2021. RNA in cancer. *Nature Reviews Cancer*, 21, 22-36.
- GRECH, N., DALLI, T., MIZZI, S., MEILAK, L., CALLEJA, N. & ZRINZO, A. 2020. Rising Incidence of Glioblastoma Multiforme in a Well-Defined Population. *Cureus*, 12, e8195.
- HANSEN, T. B., JENSEN, T. I., CLAUSEN, B. H., BRAMSEN, J. B., FINSEN, B., DAMGAARD, C. K. & KJEMS, J. 2013. Natural RNA circles function as efficient microRNA sponges. *Nature*, 495, 384-388.
- HEALTH, A. I. O. & WELFARE 2022. Cancer data in Australia. Canberra: AIHW.
- HIROSE, J., KAWASHIMA, H., YOSHIE, O., TASHIRO, K. & MIYASAKA, M. 2001. Versican interacts with chemokines and modulates cellular responses. *Journal of Biological Chemistry*, 276, 5228-5234.
- HOLDT, L. M., KOHLMAIER, A. & TEUPSER, D. 2018. Circular RNAs as therapeutic agents and targets. *Frontiers in physiology*, 9, 1262.
- HSU, M. T. & COCA-PRADOS, M. 1979. Electron microscopic evidence for the circular form of RNA in the cytoplasm of eukaryotic cells. *Nature*, 280, 339-40.
- HUANG, A., ZHENG, H., WU, Z., CHEN, M. & HUANG, Y. 2020. Circular RNA-protein interactions: functions, mechanisms, and identification. *Theranostics*, 10, 3503.
- HUANG, C., LIANG, D., TATOMER, D. C. & WILUSZ, J. E. 2018. A length-dependent evolutionarily conserved pathway controls nuclear export of circular RNAs. *Genes Dev*, 32, 639-644.

- JIN, C., ZHAO, J., ZHANG, Z. P., WU, M., LI, J., LIU, B., BIN LIAO, X., LIAO, Y. X. & LIU, J. P. 2021. CircRNA EPHB4 modulates stem properties and proliferation of gliomas via sponging miR - 637 and up - regulating SOX10. *Molecular oncology*, 15, 596-622.
- KIM, Y. S., NAKANISHI, G., LEWANDOSKI, M. & JETTEN, A. M. 2003. GLIS3, a novel member of the GLIS subfamily of Krüppel - like zinc finger proteins with repressor and activation functions. *Nucleic Acids Research*, 31, 5513-5525.
- KORESSAAR, T. & REMM, M. 2007. Enhancements and modifications of primer design program Primer3. *Bioinformatics*, 23, 1289-1291.
- KRISTENSEN, L., HANSEN, T., VENØ, M. & KJEMS, J. 2018. Circular RNAs in cancer: opportunities and challenges in the field. *Oncogene*, 37, 555-565.
- KRISTENSEN, L. S., ANDERSEN, M. S., STAGSTED, L. V., EBBESEN, K. K., HANSEN, T. B. & KJEMS, J. 2019. The biogenesis, biology and characterization of circular RNAs. *Nature Reviews Genetics*, 20, 675-691.
- LEE, S. Y. 2016. Temozolomide resistance in glioblastoma multiforme. *Genes Dis*, 3, 198-210.
- LEE, Y. J., SEO, H. W., BAEK, J. H., LIM, S. H., HWANG, S. G. & KIM, E. H. 2020. Gene expression profiling of glioblastoma cell lines depending on TP53 status after tumor-treating fields (TTFs) treatment. *Sci Rep*, 10, 12272.
- LEECE, R., XU, J., OSTROM, Q. T., CHEN, Y., KRUCHKO, C. & BARNHOLTZ -SLOAN, J. S. 2017. Global incidence of malignant brain and other central nervous system tumors by histology, 2003–2007. *Neuro-oncology*, 19, 1553-1564.
- LI, G. & LAN, Q. 2021. Exosome-Mediated Transfer of circ-GLIS3 Enhances Temozolomide Resistance in Glioma Cells Through the miR-548m/MED31 Axis. *Cancer Biotherapy and Radiopharmaceuticals*.
- LI, J., SUN, D., PU, W., WANG, J. & PENG, Y. 2020. Circular RNAs in Cancer: Biogenesis, Function, and Clinical Significance. *Trends Cancer*, 6, 319-336.

- LI, X. & DIAO, H. 2019. Circular RNA circ\_0001946 acts as a competing endogenous RNA to inhibit glioblastoma progression by modulating miR-671-5p and CDR1. *J Cell Physiol*, 234, 13807-13819.
- LI, Z., HUANG, C., BAO, C., CHEN, L., LIN, M., WANG, X., ZHONG, G., YU, B., HU, W. & DAI, L. 2015. Exon-intron circular RNAs regulate transcription in the nucleus. *Nature structural & molecular biology*, 22, 256-264.
- LIANG, D. & WILUSZ, J. E. 2014. Short intronic repeat sequences facilitate circular RNA production. *Genes & development*, 28, 2233-2247.
- LIM, M., XIA, Y., BETTEGOWDA, C. & WELLER, M. 2018. Current state of immunotherapy for glioblastoma. *Nature reviews Clinical oncology*, 15, 422-442.
- LIU, B., LIU, N., ZHU, X., YANG, L., YE, B., LI, H., ZHU, P., LU, T., TIAN, Y. & FAN, Z. 2021. Circular RNA circZbtb20 maintains ILC3 homeostasis and function via Alkbh5-dependent m6A demethylation of Nr4a1 mRNA. *Cellular & Molecular Immunology*, 18, 1412-1424.
- LIU, D., CONN, V., GOODALL, G. & CONN, S. 2018. A Highly Efficient Strategy for Overexpressing circRNAs.
- LIU, D., LIU, W., CHEN, X., YIN, J., MA, L., LIU, M., ZHOU, X., XIAN, L., LI, P. & TAN, X. 2022. circKCNN2 suppresses the recurrence of hepatocellular carcinoma at least partially via regulating miR - 520c - 3p/methyl - DNA - binding domain protein 2 axis. *Clinical and translational medicine*, 12, e662.
- LIU, Y.-T. & SUN, Z.-J. 2021. Turning cold tumors into hot tumors by improving T-cell infiltration. *Theranostics*, 11, 5365.
- LU, Z., FILONOV, G. S., NOTO, J. J., SCHMIDT, C. A., HATKEVICH, T. L., WEN, Y., JAFFREY, S. R. & MATERA, A. G. 2015. Metazoan tRNA introns generate stable circular RNAs in vivo. *Rna*, 21, 1554-1565.

- LUKE, J. J., FLAHERTY, K. T., RIBAS, A. & LONG, G. V. 2017. Targeted agents and immunotherapies: optimizing outcomes in melanoma. *Nature reviews Clinical oncology*, 14, 463-482.
- LV, K., CAO, X., WANG, R., DU, P., FU, J., GENG, D. & ZHANG, J. 2022. Neuroplasticity of Glioma Patients: Brain Structure and Topological Network. *Front Neurol*, 13, 871613.
- MAASS, P. G., GLAŽAR, P., MEMCZAK, S., DITTMAR, G., HOLLFINGER, I., SCHREYER, L., SAUER, A. V., TOKA, O., AIUTI, A. & LUFT, F. C. 2017. A map of human circular RNAs in clinically relevant tissues. *Journal of molecular medicine*, 95, 1179-1189.
- MARQUET, G., DAMERON, O., SAIKALI, S., MOSSER, J. & BURGUN, A. 2007. Grading glioma tumors using OWL-DL and NCI Thesaurus. *AMIA Annu Symp Proc*, 2007, 508-12.
- MCDERMAID, A., MONIER, B., ZHAO, J., LIU, B. & MA, Q. 2019. Interpretation of differential gene expression results of RNA-seq data: review and integration. *Briefings in bioinformatics*, 20, 2044-2054.
- MCKINNON, C., NANDHABALAN, M., MURRAY, S. A. & PLAHA, P. 2021. Glioblastoma: clinical presentation, diagnosis, and management. *Bmj*, 374.
- MEDICINE, N. L. O. 2023. LRFN1 leucine rich repeat and fibronectin type III domain containing 1 [ Homo sapiens (human) ].
- MEMCZAK, S., JENS, M., ELEFSINIOTI, A., TORTI, F., KRUEGER, J., RYBAK, A., MAIER, L., MACKOWIAK, S. D., GREGERSEN, L. H. & MUNSCHAUER, M. 2013. Circular RNAs are a large class of animal RNAs with regulatory potency. *Nature*, 495, 333-338.
- MÜLLER, S. & APPEL, B. 2017. In vitro circularization of RNA. *RNA biology*, 14, 1018-1027.
- NIELSEN, A. F., BINDEREIF, A., BOZZONI, I., HANAN, M., HANSEN, T. B., IRIMIA, M., KADENER, S., KRISTENSEN, L. S., LEGNINI, I. & MORLANDO, M. 2022. Best practice standards for circular RNA research. *Nature Methods*, 19, 1208-1220.

- OHTA, S., HAMADA, M., SATO, N. & TORAMOTO, I. 2015. Polyglutamylated Tubulin Binding Protein C1orf96/CSAP Is Involved in Microtubule Stabilization in Mitotic Spindles. *PLoS One*, 10, e0142798.
- OSTROM, Q. T., BAUCHET, L., DAVIS, F. G., DELTOUR, I., FISHER, J. L., LANGER, C. E., PEKMEZCI, M., SCHWARTZBAUM, J. A., TURNER, M. C., WALSH, K. M., WRENSCH, M. R. & BARNHOLTZ-SLOAN, J. S. 2014. The epidemiology of glioma in adults: a "state of the science" review. *Neuro Oncol*, 16, 896-913.
- OSTROM, Q. T., GITTLEMAN, H., TRUITT, G., BOSCIA, A., KRUCHKO, C. & BARNHOLTZ-SLOAN, J. S. 2018. CBTRUS statistical report: primary brain and other central nervous system tumors diagnosed in the United States in 2011–2015. *Neuro-oncology*, 20, iv1-iv86.
- PAN, Z., CAI, J., LIN, J., ZHOU, H., PENG, J., LIANG, J., XIA, L., YIN, Q., ZOU, B., ZHENG, J., QIAO, L. & ZHANG, L. 2020. A novel protein encoded by circFND3B inhibits tumor progression and EMT through regulating Snail in colon cancer. *Mol Cancer*, 19, 71.
- PIWECKA, M., GLAŽAR, P., HERNANDEZ-MIRANDA, L. R., MEMCZAK, S., WOLF, S. A., RYBAK-WOLF, A., FILIPCHYK, A., KLIRONOMOS, F., CERDA JARA, C. A. & FENSKE, P. 2017. Loss of a mammalian circular RNA locus causes miRNA deregulation and affects brain function. *Science*, 357, eaam8526.
- REN, M., SONG, X., NIU, J., TANG, G., SUN, Z., LI, Y. & KONG, F. 2022. The malignant property of circHIPK2 for angiogenesis and chemoresistance in non-small cell lung cancer. *Experimental Cell Research*, 419, 113276.
- RYKEN, T. C., AYGUN, N., MORRIS, J., SCHWEIZER, M., NAIR, R., SPRACKLEN, C., KALKANIS, S. N. & OLSON, J. J. 2014. The role of imaging in the management of progressive glioblastoma. *Journal of Neuro-oncology*, 118, 435-460.
- SALAMI, R., SALAMI, M., MAFI, A., VAKILI, O. & ASEMI, Z. 2022. Circular RNAs and glioblastoma multiforme: focus on molecular mechanisms. *Cell Commun Signal*, 20, 13.

- SALZMAN, J., GAWAD, C., WANG, P. L., LACAYO, N. & BROWN, P. O. 2012. Circular RNAs are the predominant transcript isoform from hundreds of human genes in diverse cell types. *PloS one*, 7, e30733.
- SAMUELS-LEV, Y., O'CONNOR, D. J., BERGAMASCHI, D., TRIGIANTE, G., HSIEH, J.-K., ZHONG, S., CAMPARGUE, I., NAUMOVSKI, L., CROOK, T. & LU, X. 2001. ASPP proteins specifically stimulate the apoptotic function of p53. *Molecular cell*, 8, 781-794.
- SCHMIDT, C., NOTO, J., FILONOV, G. & MATERA, A. 2016. A method for expressing and imaging abundant, stable, circular RNAs in vivo using tRNA splicing. *Methods in enzymology*. Elsevier.
- SETO, A. G., BEATTY, X., LYNCH, J. M., HERMRECK, M., TETZLAFF, M., DUVIC, M. & JACKSON, A. L. 2018. Cobomarsen, an oligonucleotide inhibitor of miR - 155, co - ordinally regulates multiple survival pathways to reduce cellular proliferation and survival in cutaneous T - cell lymphoma. *British journal of haematology*, 183, 428-444.
- SHAFABAKHSH, R. & ASEMI, Z. 2019. Quercetin: a natural compound for ovarian cancer treatment. *Journal of ovarian research*, 12, 1-9.
- SHEN, X., WEI, Y., YOU, G., LIU, W., AMEVOR, F. K., ZHANG, Y., HE, H., MA, M., ZHANG, Y. & LI, D. 2021. Circular PPP1R13B RNA promotes chicken skeletal muscle satellite cell proliferation and differentiation via targeting miR-9-5p. *Animals*, 11, 2396.
- SHIRAISHI, F., VISNER, G. A., NICK, H. S. & AGARWAL, A. 2001. Geneticin induces endogenous heme oxygenase-1 expression: Implication in transfection studies. *Analytical Biochemistry*, 289, 303-305.
- SIM, H.-W., NOWAK, A. K., LWIN, Z. & KHASRAW, M. 2020. Management of glioblastoma: an Australian perspective. *Chinese Clinical Oncology*, 10, 42.
- SMIGIEL, R., SHERMAN, D. L., RYDZANICZ, M., WALCZAK, A., MIKOLAJKOW, D., KROLAK-OLEJNIK, B., KOSIŃSKA, J., GASPEROWICZ, P., BIERNACKA, A. & STAWINSKI, P. 2018. Homozygous mutation in the Neurofascin gene affecting the glial isoform of

- Neurofascin causes severe neurodevelopment disorder with hypotonia, amimia and areflexia. *Human molecular genetics*, 27, 3669-3674.
- STEPANENKO, A. A. & HENG, H. H. 2017. Transient and stable vector transfection: Pitfalls, off-target effects, artifacts. *Mutat Res Rev Mutat Res*, 773, 91-103.
- STUPP, R., MASON, W. P., VAN DEN BENT, M. J., WELLER, M., FISHER, B., TAPHOORN, M. J., BELANGER, K., BRANDES, A. A., MAROSI, C. & BOGDHANN, U. 2005. Radiotherapy plus concomitant and adjuvant temozolomide for glioblastoma. *New England journal of medicine*, 352, 987-996.
- SU, C. H., D, D. & TARN, W. Y. 2018. Alternative Splicing in Neurogenesis and Brain Development. *Front Mol Biosci*, 5, 12.
- TAKAO-RIKITSU, E., MOCHIDA, S., INOUE, E., DEGUCHI-TAWARADA, M., INOUE, M., OHTSUKA, T. & TAKAI, Y. 2004. Physical and functional interaction of the active zone proteins, CAST, RIM1, and Bassoon, in neurotransmitter release. *The Journal of cell biology*, 164, 301-311.
- TAN, A. C., ASHLEY, D. M., LÓPEZ, G. Y., MALINZAK, M., FRIEDMAN, H. S. & KHASRAW, M. 2020. Management of glioblastoma: State of the art and future directions. *CA Cancer J Clin*, 70, 299-312.
- TRINCZEK, B., BRAJENOVIC, M., EBNETH, A. & DREWES, G. 2004. MARK4 is a novel microtubule-associated proteins/microtubule affinity-regulating kinase that binds to the cellular microtubule network and to centrosomes. *J Biol Chem*, 279, 5915-23.
- UNTERGASSER, A., CUTCUTACHE, I., KORESSAAR, T., YE, J., FAIRCLOTH, B. C., REMM, M. & ROZEN, S. G. 2012. Primer3—new capabilities and interfaces. *Nucleic acids research*, 40, e115-e115.
- VALERO, R., MARFANY, G., GONZÁLEZ-ANGULO, O., GONZÁLEZ-GONZÁLEZ, G., PUELLES, L. & GONZÁLEZ-DUARTE, R. 1999. USP25, a novel gene encoding a deubiquitinating enzyme, is located in the gene-poor region 21q11.2. *Genomics*, 62, 395-405.

- VILLA, F., DEAK, M., BLOOMBERG, G. B., ALESSI, D. R. & VAN AALTEN, D. M. 2005. Crystal structure of the PTPL1/FAP-1 human tyrosine phosphatase mutated in colorectal cancer: evidence for a second phosphotyrosine substrate recognition pocket. *J Biol Chem*, 280, 8180-7.
- VO, J. N., CIESLIK, M., ZHANG, Y., SHUKLA, S., XIAO, L., ZHANG, Y., WU, Y.-M., DHANASEKARAN, S. M., ENGELKE, C. G. & CAO, X. 2019. The landscape of circular RNA in cancer. *Cell*, 176, 869-881. e13.
- WANG, H., CHEN, S., WEI, J., SONG, G. & ZHAO, Y. 2020. A-to-I RNA Editing in Cancer: From Evaluating the Editing Level to Exploring the Editing Effects. *Front Oncol*, 10, 632187.
- WANG, R., ZHANG, S., CHEN, X., LI, N., LI, J., JIA, R., PAN, Y. & LIANG, H. 2018. CircNT5E acts as a sponge of miR-422a to promote glioblastoma tumorigenesis. *Cancer research*, 78, 4812-4825.
- WANG, X., CHEN, J. X., LIU, J. P., YOU, C., LIU, Y. H. & MAO, Q. 2014. Gain of function of mutant TP53 in glioblastoma: prognosis and response to temozolomide. *Ann Surg Oncol*, 21, 1337-44.
- WESTBROOK, T. F., HU, G., ANG, X. L., MULLIGAN, P., PAVLOVA, N. N., LIANG, A., LENG, Y., MAEHR, R., SHI, Y., HARPER, J. W. & ELLEDGE, S. J. 2008. SCFbeta-TRCP controls oncogenic transformation and neural differentiation through REST degradation. *Nature*, 452, 370-4.
- WU, X., XIAO, S., ZHANG, M., YANG, L., ZHONG, J., LI, B., LI, F., XIA, X., LI, X. & ZHOU, H. 2021. A novel protein encoded by circular SMO RNA is essential for Hedgehog signaling activation and glioblastoma tumorigenicity. *Genome biology*, 22, 1-29.
- XIAO, M. S. & WILUSZ, J. E. 2019. An improved method for circular RNA purification using RNase R that efficiently removes linear RNAs containing G-quadruplexes or structured 3' ends. *Nucleic Acids Res*, 47, 8755-8769.

- XIAO, W., LI, J., HU, J., WANG, L., HUANG, J. R., SETHI, G. & MA, Z. 2021. Circular RNAs in cell cycle regulation: Mechanisms to clinical significance. *Cell proliferation*, 54, e13143.
- XIN, J., ZHANG, X., SUN, D., TIAN, L. & XU, P. 2019. Up-regulated circular RNA hsa\_circ\_0067934 contributes to glioblastoma progression through activating PI3K-AKT pathway. *Eur Rev Med Pharmacol Sci*, 23, 3447-3454.
- YANG, Q., LI, F., HE, A. T. & YANG, B. B. 2021. Circular RNAs: Expression, localization, and therapeutic potentials. *Molecular Therapy*, 29, 1683-1702.
- YANG, Y., FAN, X., MAO, M., SONG, X., WU, P., ZHANG, Y., JIN, Y., YANG, Y., CHEN, L.-L. & WANG, Y. 2017. Extensive translation of circular RNAs driven by N6-methyladenosine. *Cell research*, 27, 626-641.
- YOU, X., VLATKOVIC, I., BABIC, A., WILL, T., EPSTEIN, I., TUSHEV, G., AKBALIK, G., WANG, M., GLOCK, C. & QUEDENAU, C. 2015. Neural circular RNAs are derived from synaptic genes and regulated by development and plasticity. *Nature neuroscience*, 18, 603-610.
- ZHANG, F., NAKANISHI, G., KUREBAYASHI, S., YOSHINO, K., PERANTONI, A., KIM, Y.-S. & JETTEN, A. M. 2002. Characterization of Glis2, a Novel Gene Encoding a Gli-related, Krüppel-like Transcription Factor with Transactivation and Repressor Functions: Roles in Kidney Development and Neurogenesis. *Journal of Biological Chemistry*, 277, 10139-10149.
- ZHANG, S., LIAO, K., MIAO, Z., WANG, Q., MIAO, Y., GUO, Z., QIU, Y., CHEN, B., REN, L. & WEI, Z. 2019. CircFOXO3 promotes glioblastoma progression by acting as a competing endogenous RNA for NFAT5. *Neuro-oncology*, 21, 1284-1296.
- ZHANG, W., MI, J., LI, N., SUI, L., WAN, T., ZHANG, J., CHEN, T. & CAO, X. 2001. Identification and characterization of DPZF, a novel human BTB/POZ zinc finger protein sharing homology to BCL-6. *Biochem Biophys Res Commun*, 282, 1067-73.

- ZHANG, X.-O., WANG, H.-B., ZHANG, Y., LU, X., CHEN, L.-L. & YANG, L. 2014. Complementary Sequence-Mediated Exon Circularization. *Cell*, 159, 134-147.
- ZHANG, Y., LIN, X., GENG, X., SHI, L., LI, Q., LIU, F., FANG, C. & WANG, H. 2020. Advances in circular RNAs and their role in glioma. *International Journal of Oncology*, 57, 67-79.
- ZHANG, Y., ZHANG, X.-O., CHEN, T., XIANG, J.-F., YIN, Q.-F., XING, Y.-H., ZHU, S., YANG, L. & CHEN, L.-L. 2013. Circular intronic long noncoding RNAs. *Molecular cell*, 51, 792-806.
- ZHOU, W. Y., CAI, Z. R., LIU, J., WANG, D. S., JU, H. Q. & XU, R. H. 2020. Circular RNA: metabolism, functions and interactions with proteins. *Mol Cancer*, 19, 172.
- ZHU, L. W. & LIU, L. 2019. Retraction: Circular RNA - 0007874 (circMTO1) reverses chemoresistance to temozolomide by acting as a sponge of microRNA - 630 in glioblastoma by Jiang Rao, Xinxin Cheng, Huimin. *Cell Biol Int*, 1.